Geochimica et Cosmochimica Acta 394 (2025) 220–243

Contents lists available at ScienceDirect

Geochimica et Cosmochimica Acta

journal homepage: www.elsevier.com/locate/gca

Extreme enriched-mantle (EM) compositions recorded by the Sr-Nd-Hf isotopes of global cratonic lamproites

Soumendu Sarkar [a,b,d,*], Hayden Dalton [a], Andrea Giuliani [c,j], David Phillips [a], D. Graham Pearson [d], Geoff M. Nowell [e], Jon D. Woodhead [a], Janet Hergt [a], Roland Maas [a], A. Lynton Jaques [f], N.V. Chalapathi Rao [g,h], Yaakov Weiss [i], Sujoy Ghosh [b]

[a] School of Geography, Earth and Atmospheric Sciences, The University of Melbourne, Parkville 3010 Victoria, Australia
[b] Department of Geology and Geophysics, Indian Institute of Technology Kharagpur, Kharagpur, West Bengal 721302, India
[c] Institute of Geochemistry and Petrology, Department of Earth Sciences, ETH Zurich, Clausiusstrasse 25, 8092 Zurich, Switzerland
[d] Department of Earth and Atmospheric Sciences, University of Alberta, 1-26 Earth Sciences Building, Edmonton, AB T6G 2E3, Canada
[e] Department of Earth Sciences, University of Durham, Durham DH1 3LE, UK
[f] Research School of Earth Sciences, Australian National University, Canberra ACT 2000, Australia
[g] Mantle Petrology Laboratory, Department of Geology, Institute of Science, Banaras Hindu University, Varanasi 221005, India
[h] National Centre for Earth Science Studies, Akkulam, Thiruvanathapuram 695011, India
[i] Institute of Earth Sciences, The Hebrew University of Jerusalem, Jerusalem 91904, Israel
[j] Earth and Planets Laboratory, Carnegie Institution for Science, Washington 20015 DC, United States

ARTICLE INFO

Associate editor: Dmitri A. Ionov

Keywords:
Lamproites
Sr-Nd-Hf isotopes
Lithospheric mantle
Kimberlites
Ocean Island basalt

ABSTRACT

Cratonic lamproites are rare ultrapotassic rocks that occur in every continent and were emplaced over the last 2 billion years. Owing to their highly radiogenic Sr and unradiogenic Nd-Hf isotopic compositions along with enrichment in K and incompatible trace elements (e.g., Ba, Sr, Ti, Zr), lamproites are believed to be formed by melting geochemically enriched regions in the sub-continental lithospheric mantle (SCLM). In contrast, olivine compositions indistinguishable from those of kimberlites and the occurrence of diamonds containing inclusions of majorite-bearing garnet in some cratonic lamproites, suggest that primary lamproitic (or proto-lamproitic) melts may originate in the convecting mantle. Here we re-evaluate the different source component(s) responsible for the genesis of cratonic lamproites worldwide using major-, trace-element and radiogenic isotope geochemistry.

We report new major-, trace-element and Sr, Nd and Hf isotope compositions for 61 cratonic lamproite samples from sixteen cratons, with an emphasis on localities lacking Hf isotope data. These data, combined with published results, reveal three discernible end-member compositions in Sr-Nd-Hf isotope space. The first end-member includes lamproites with the least geochemically-enriched isotopic signatures (i.e. less radiogenic Sr, less negative and locally positive εNd and εHf values) (e.g., Wajrakarur and Bunder in India, Melville in Canada), similar to the Bulk Silicate Earth (BSE), which overlap with those of global ocean island basalts (OIBs) and archetypal kimberlites. The second end-member is represented by the Cenozoic West Kimberley lamproites (Australia), which exhibit the highest εSr values with low εNd and εHf compositions and resemble EM II OIBs from Samoa. The third end-member, defined by lamproites from Leucite Hills and Smoky Butte (USA), exhibits strongly negative εNd and εHf values, associated with moderately negative εSr compositions similar to, although more extreme than, EM I OIBs. The remaining lamproites included in this study have intermediate isotopic compositions that fall between these three end-members. The similar Sr-Nd-Hf compositions of the least geochemically enriched lamproites, OIBs and kimberlites suggest a predominant input from the convective mantle for these lamproites. Conversely, the lamproites with more geochemically enriched Sr-Nd-Hf isotopic compositions (i.e. more radiogenic Sr, more negative εNd and εHf values) necessitate extreme source compositions that, locally, cannot be accounted for by commonly observed mantle components, such as lithospheric mantle xenoliths dominated by mica (e.g., MARID) or subducted crust/sediment. Theoretical components generated by long-term enrichment of the lithospheric mantle mediated by subduction-related fluids appear to be required to produce mica-bearing peridotites that, with time, develop isotopic compositions similar to those

* Corresponding author.
E-mail address: soumendu@ualberta.ca (S. Sarkar).

https://doi.org/10.1016/j.gca.2025.02.014
Received 12 November 2024; Accepted 12 February 2025
Available online 22 February 2025

observed in the most geochemically enriched lamproites. The spread in isotopic compositions observed in lamproites from some regions (e.g., Cenozoic West Kimberley) is best explained via assimilation of anciently metasomatised lithospheric mantle peridotites by melts derived from moderately depleted convective mantle sources rather than exclusive melting of lithospheric mantle sources. Differences in the proportions of various end-members, combined with the diverse isotopic compositions of metasomatized SCLM across different regions and at different times are crucial in creating the unique mineralogical and isotopic characteristics documented in lamproites from each province. Thus, cratonic lamproites offer insights into the cratonic lithosphere and its metasomatic evolution.

1. Introduction

Cratonic lamproites (equivalent to "anorogenic" lamproites; e.g. Prelević et al. 2008) represent some of the most potassium-rich and deepest-derived magmas on Earth, locally incorporating abundant lithospheric mantle material (including diamonds) as they ascend toward the surface. These alkaline rocks are relatively rare even when compared to other diamondiferous magmas such as archetypal kimberlites (low-volume ultramafic rocks enriched in volatiles (H_2O and/or CO_2) and incompatible trace elements; Pearson et al., 2019) and are found in fewer than 50 provinces across all continents (Mitchell, 2020). Cratonic lamproites are host to major diamond mines in Australia (Argyle, Ellendale) and South Africa (Finsch, Voorspoed), with the Argyle AK1 Mine being one of the world's highest-grade primary diamond deposits, yielding up to 680 ct/100 t (Kjarsgaard et al., 2022). In terms of mantle geochemistry, their composition is important for understanding the diverse nature of the lithospheric mantle and enrichment processes thereof (e.g., Fraser and Hawkesworth, 1992; Tainton and McKenzie, 1994; Becker and Le Roex, 2006). Thus, lamproites are both economically and scientifically important.

Lamproite magmas generally display extrusive forms with few examples of intrusive bodies (Mitchell and Bergman, 1991; Mitchell, 2020, 2021). These include subaerial lava flows, lava lakes, cinder cones, lithified pyroclastic deposits, differentiated sills, and dike swarms. Cratonic lamproites with coherent (i.e. non-clastic) texture are inequigranular, with abundant phlogopite and subordinate olivine macrocrysts (including xenocrysts) and microcrysts, embedded in a groundmass comprising abundant phlogopite, diopside, apatite, spinel, minor perovskite, and, in some cases, calcite (and/or dolomite), with the addition of K-richterite in more evolved varieties and Ti-rich phases (e.g., priderite, wadeite) in some Ti-rich lamproites (e.g., Mitchell and Bergman, 1991; Mitchell, 1995). Geochemically, cratonic lamproites are peralkaline [molar $(K_2O + Na_2O)/Al_2O_3 > 1$] and ultrapotassic (molar $K_2O/Na_2O > 3$), with varying CO_2 and H_2O contents (Mitchell and Bergman, 1991; Pearson et al., 2019). They also exhibit strong enrichment in large ion lithophile elements (LILE) (e.g. K, Rb, Ba, Sr), and light rare earth elements (LREEs) with characteristic negative Ti anomalies (Fraser et al., 1985; Nelson et al., 1986; Woolley et al., 1996; Becker and Le Roex, 2006; Pearson et al., 2019). In contrast, kimberlites differ from cratonic lamproites by the absence of feldspar, feldspathoids, clinopyroxene, and amphiboles of any kind (Mitchell et al., 2020). Additionally, kimberlites are richer in MgO (mean MgO ~ 30.2 wt%) and characterized by higher CO_2 content (up to 30 wt%) compared to lamproites (mean MgO ~ 22.53 wt% and CO_2 up to 22 wt%), with relatively low levels of K, Na, and Al, and exceptionally low Na content (<0.1 wt% Na_2O), with molar $(Na_2O + K_2O)/Al_2O_3 < 1$ (Kjarsgaard et al., 2022; Giuliani et al. 2020, 2024). While cratonic lamproites are less abundant compared to kimberlites, they have been sporadically emplaced across different cratons over the last 2 Ga (Fig. 1; n = 229, Supplementary Table 1a; also see Kjarsgaard et al., 2022). The oldest known lamproites are the Paleoproterozoic Brockman Creek intrusions in Australia, dating back to 1920 Ma (Wyatt et al., 1998), whereas the most recent is the Gaussberg olivine lamproite in Antarctica, estimated to be 56,000 years old (Tingey et al., 1983).

Previous research has led to suggestions that cratonic lamproites may arise from partial melting of hydrous veins, such as MARIDs (mica-amphibole-rutile-ilmenite-diopside bearing rocks), in peridotites or phlogopite-rich peridotites (Fraser et al., 1985; Foley et al., 1987; Foley, 1992; Mitchell, 1995; Giuliani et al., 2015). Derivation from a metasomatized mica-bearing sub-continental lithospheric mantle (SCLM) source is supported by elevated K, enrichment in incompatible trace elements, highly radiogenic Sr and unradiogenic Nd isotope compositions (metasomatized mica-bearing SCLM includes not only mica but also other metasomatic phases such as amphibole and clinopyroxene, where unradiogenic Nd would be stored) (McCulloch et al., 1983; Smith, 1983; Jaques et al., 1984; Fraser et al., 1985; Nelson et al., 1986; Mitchell and Bergman, 1991; Mitchell, 1995, 2020; Nowell et al., 1998; Becker and Le Roex, 2006; Coe et al., 2008; Pearson et al., 2019). They differ from archetypal kimberlites which have lower K and higher CO_2 contents and more geochemically depleted Sr and Nd isotope compositions, consistent with derivation from convecting sub-lithospheric mantle sources (Smith, 1983; Nowell et al., 2004; Becker and Le Roex, 2006; Pearson et al., 2019; Woodhead et al., 2019; Giuliani et al., 2024).

Recent work has recognised that an origin by partial melting of the lithospheric mantle is complicated by strict geodynamic requirements related to increasing geothermal gradients for example via lithospheric thinning or mantle plume impingement (e.g. Phillips et al., 1998; Chalapathi Rao and Lehmann, 2011). An alternative model entails contributions of heat and additional geochemical components by ascending melts from the convecting mantle which interact with phlogopite-rich metasomatic domains in the SCLM (generally up to ~200–250 km thickness) to form lamproites (Shaikh et al., 2018; Sarkar et al., 2021, 2022). Evidence supporting the involvement of a sub-lithospheric mantle source include: i) the presence of majorite-bearing garnet (stable below ~250 km in the convective mantle) inclusions in the sub-lithospheric diamonds of some cratonic lamproites (Stachel et al., 2018), ii) similar olivine compositional systematics in cratonic lamproites and kimberlites worldwide (Sarkar et al., 2022); iii) indistinguishable isotopic signatures for lamproites and kimberlites in the Wajrakarur field (Paton et al., 2009; Chalapthi Rao et al., 2013; Giuliani et al., 2022), and iv) correlations between emplacement ages and isotopic compositions in adjacent kimberlites and lamproites in the Kaapvaal craton, which point to common evolving sources in the convective mantle (Sarkar et al., 2023). These lines of evidence suggest that primary lamproitic (or proto-lamproitic) melts may also originate in the convective mantle as proposed in some previous studies (Murphy et al., 2002; Jaques et al., 2018). Further investigation is necessary to ascertain whether this sub-lithospheric (convective) mantle contribution is ubiquitous in the source of global cratonic lamproites, as previously proposed for K-rich ultramafic lamprophyres (Tappe et al., 2008; Dalton et al., 2019, 2022; Giuliani et al., 2017; Wang et al., 2021, 2022).

The aim of this study is to integrate new and existing Sr-Nd-Hf isotope data from worldwide cratonic lamproites, combined with major and trace element results, to contribute to the ongoing discourse on the origin of these unusual magmas. Although numerous studies have determined the Sr and Nd isotope compositions of cratonic lamproites from several regions (e.g., Kaapvaal, West Kimberley), there is a noticeable lack of Hf isotope analyses (see Supplementary Table 1a). Hafnium isotopes, combined with Nd and Sr isotopes, can provide powerful insights into the nature of geochemically-enriched (defined by

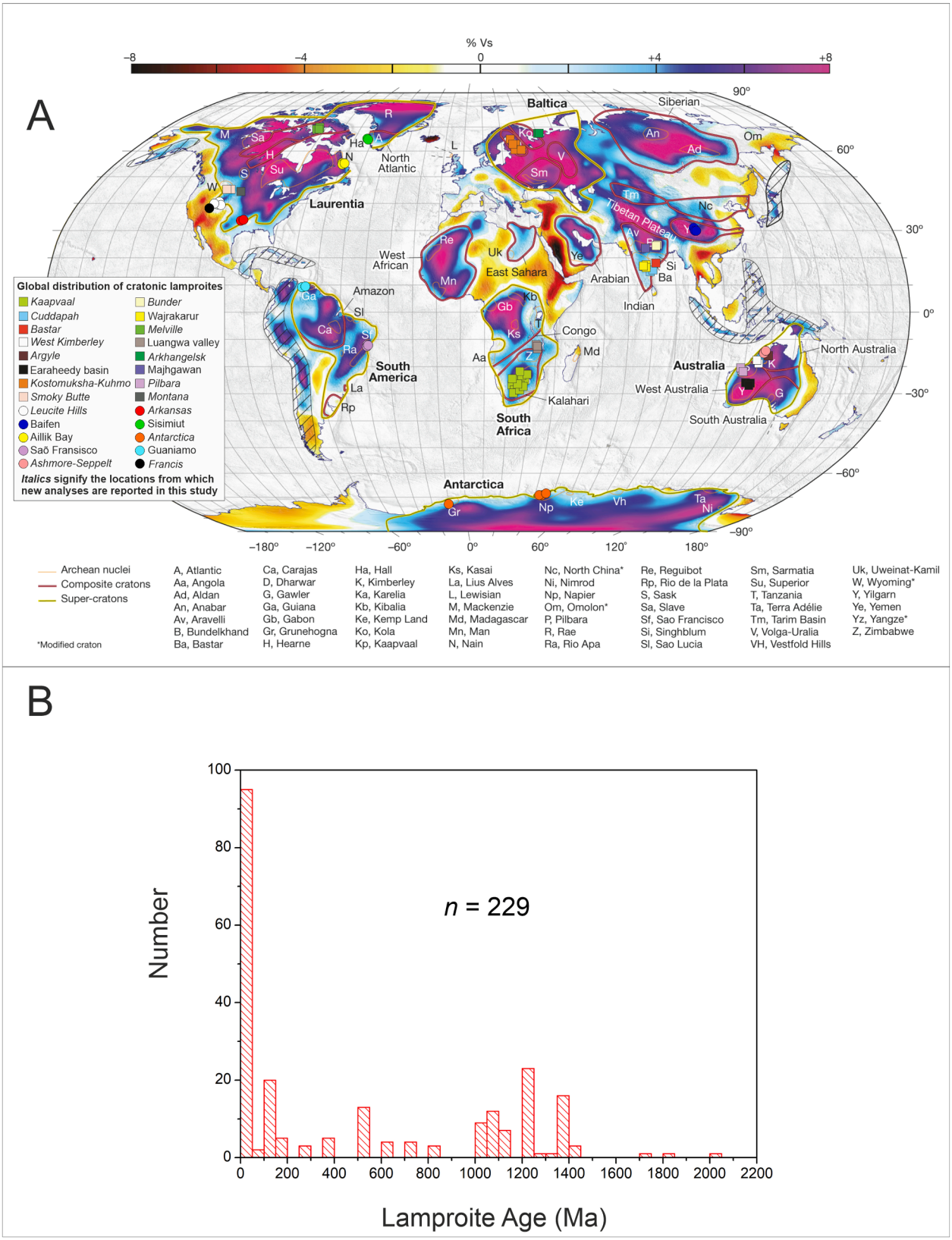

Fig. 1. (a) Global distribution of lamproites (colored rectangles and circles) showing sample localities examined in this study (global S-wave tomography map (based on AK135 reference model) modified from Pearson et al. 2021) and (b) frequency distribution of cratonic lamproites (n = 229; bin = 50 Ma; Oversampled data for the same intrusion/pipe are identified based on sample codes or names in the compilation. In the case of several analyses available for a single location, we have only considered them as a single data point in the frequency distribution; see description in Supplementary Table 1). Sample attributes are summarised in Supplementary Table 1.

more radiogenic Sr, more negative εNd and εHf values) components in the mantle including, for example, deeply subducted oceanic crust (e.g., Blichert-Toft et al., 1999; Nowell et al., 2004; Chauvel et al., 2008; Nebel et al., 2013; Dalton et al., 2022), hence improving knowledge of lamproite genesis. Here, we present new Sr-Nd-Hf isotopic, major, and trace element compositions for 61 fresh lamproite samples with ages ranging between 2 Ga and the Quaternary, and compare these results with an exhaustive compilation of existing data for cratonic lamproites worldwide. We then use the combined data-set to re-evaluate the origin of cratonic lamproites on a global scale. Specifically, we seek to identify specific source components (lithospheric or asthenospheric) included in lamproite melts as well as the mantle processes (e.g., lithospheric assimilation, deep subduction, metasomatism) that might have contributed to the observed isotopic variations in these rocks.

2. Samples and petrography

Sample selection was based on addressing the paucity of Hf isotope data while also canvassing as many lamproite provinces as possible (Fig. 1a). Sixteen samples were collected from the Kaapvaal craton (Newlands, New Elands, Finsch, Klipspringer, Robert Victor, Sanddrift, Star, Markt, Bestershoek, Sover; collectively considered as Kaapvaal lamproites due to their consistent chemistry and similar Cretaceous age). Nine of the lamproite samples were sourced from India: Sakri (n = 2), Behradih (n = 1) and Kodomali (n = 1) from the Bastar craton (we have collectively considered them as Bastar lamproites because of their overall similar geochemistry; see below), Bunder/Atri (n = 2) from the Bundelkhand craton, Garledinne (n = 1) and Krishna (n = 2) from the Cuddapah basin. Additional samples are from Cenozoic West Kimberley (n = 4), Neoproterozoic Ashmore-Seppelt (n = 3) and Mesoproterozoic Argyle (n = 2) in the West Kimberley craton, Australia, Brockman Creek in the Pilbara craton (n = 2; Australia), Smoky Butte (n = 5) and Bear Gulch lamproites locating near the Montana-Florida lineament (n = 2) in Montana, Leucite Hills in the Wyoming craton (n = 6), Francis (n = 1) in Utah, Prairie Creek in the Arkansas (n = 3; all in USA), Aviat (Melville) in the Rae craton (n = 2; Canada), Kostomukhsha (n = 2; Russia) and Arkhangelsk (n = 2; Russia) in the Kola craton, and Gaussberg in Antarctica (n = 2). The majority of the samples consisted of hand specimens including a few drill core fragments. Notably, the Krishna (n = 2) and Gaussberg (n = 2) samples were available exclusively as powders. When several rock samples were available, our selection was directed toward the least altered material, determined (where possible) through careful microscopic observations. All the studied samples are sourced from existing collections, some of which have been utilised in previous studies and here we look to augment that existing data.

The lamproite samples examined in this study typically exhibit an inequigranular texture consisting of variably altered olivine macrocrysts (>1 mm) and microcrysts (<1 mm) set in fine-grained matrix. The groundmass is composed of a diverse combination of phlogopite, diopside and, in some cases, K-richterite with minor spinel and apatite along with accessory minerals such as perovskite, leucite, armalcolite, analcite, sanidine, glass, and priderite. Characteristics that differ from these 'common' features are summarised for each locality below.

Of the 61 samples studied, only the Cenozoic West Kimberley and Leucite Hills lamproites contain leucite in the groundmass. The Smoky Butte lamproite samples have a groundmass consisting of olivine, phlogopite, diopside, armalcolite, analcite, sanidine, glass, K-richterite, priderite, and apatite. Those from Prairie Creek (Arkansas) feature a groundmass composed of phlogopite, K-richterite, and glass. The Kaapvaal lamproites are characterized by the presence of large olivine macrocrysts (and minor garnet) with microcrysts of olivine, phlogopite, and diopside, set in a groundmass of phlogopite, clinopyroxene, calcite, serpentine, and apatite; these samples lack K-richterite in the groundmass. The Ashmore-Seppelt samples contain completely altered olivine macrocrysts and microcrysts replaced by serpentine, chlorite, and carbonate. The groundmass comprises abundant orange-brown tetraferriphlogopite-rich mica, chromite, Fe-Ti-rich spinel, ilmenite and calcite, with the Ashmore samples also hosting groundmass rutile. In the Seppelt samples, perovskite and rare diopside are present as additional phases. The Brockman Creek samples contain olivine macrocrysts and microcrysts, completely replaced by carbonate and minor serpentine, set in a groundmass comprising red and brown-orange tetraferriphlogopite-rich mica, carbonate and spinel. Although Ashmore, Seppelt and Brockman Creek were previously considered to be kimberlites (Wyatt et al., 1998; Reddicliffe et al., 2003), these petrographic observations and the geochemical features presented below indicate that these samples are cratonic lamproites.

2.1. Global compilation

Isotopic data for global lamproites (Supplementary Table 1a) were compiled using available literature. The global lamproite major and trace element database (Supplementary Table 1b) is an updated version of the previous compilation by Giuliani et al. (2024), supplemented with additional data extracted from individual publications. We have selected only lamproite samples that are described in the literature as fresh, relatively fresh, or minimally altered, whenever these details are available. The full list of references utilised to compile the dataset used in this study is compiled in Supplementary Table 1. It is important to note that lamproite nomenclature has been complicated by numerous type-locality names, making it difficult to identify similarities and determine which locations to include in our compilation. The confusion in lamproite terminology arose from the earlier understanding that diamonds were exclusive to kimberlites. Smith (1983) classified southern African kimberlites into Group I and Group II, linked to "basaltic" and "micaceous" varieties. Although the term "basaltic" was later abandoned, the "micaceous" label persisted. Mitchell (1986) grouped all kimberlites together, but Dawson (1980) suggested that southern African Group II kimberlites resembled lamproites. Mitchell (1995) later renamed micaceous/Group II kimberlites as "orangeites" suggesting they were unique to southern Africa. However, Mahotkin (1998) and O'Brien and Tyni (1999) identified similar rocks in Finland and western Russia. Recently, Pearson et al. (2019) resolved these nomenclature issues and the orangeite vs lamproite 'debate' by using "kimberlite" instead of Group I kimberlite and introducing the term "carbonate-rich olivine lamproite" (CROL) for rocks formerly known as micaceous kimberlite, Group II kimberlite or orangeite. We have used this classification scheme in this work and we include carbonate-rich as well as carbonate-poor lamproites in our global compilation of micaceous rocks from cratonic and pericratonic settings and collectively term them "cratonic lamproites". Additionally, while some locations (~20% of the total bulk chemistry data in Supplementary Table 1b) are not ultrapotassic (i.e., molar $K_2O/Na_2O < 3$), which contradicts the general definition of lamproites as ultrapotassic, we have included them in this study. This is because they were previously classified as lamproites based on their mica and spinel mineral chemistry, as well as their overall petrography (see Mitchell, 2020, 2021).

3. Analytical Methods

3.1. Sample preparation

Rock fragments and segments of drill-core were carefully chosen based on freshness and the absence of visible xenoliths. These samples were then crushed using a steel jaw crusher. Small chips (<1 cm) representing the freshest material (generally dark and shiny micaceous fragments) were meticulously selected under a binocular microscope. This material was then powdered using agate mills at the University of Melbourne, Durham University, and ETH Zürich in preparation for whole-rock major-, trace-element and isotopic analyses (Table 1).

Table 1
Summary of sample analyses.

Sample number	Locality/sample code	Field/cluster/province	XRF analysis	Trace element analysis	Isotope analysis	Previous isotope data available
SL1	Bu-305A	Bunder (India)	Yes[a]	Yes[b]	bulk Hf[b]	bulk Sr-Nd
SL2	Bu-PQ11	Bunder (India)	Yes[a]	Yes[b]	bulk Sr-Nd-Hf[b]	
SL3	Kos-98–5	Kostomukhsha (Russia)	Yes[a]	Yes[b]	bulk Sr-Nd-Hf[b]	
SL4	Kos-Ol	Kostomukhsha (Russia)	Yes[a]	Yes[b]	bulk Sr-Nd-Hf[b]	
SL5	PRCL-1	Prairie Creek (USA)	Yes[a]	Yes[b]	bulk Sr-Nd-Hf[b]	
SL6	PRCL-2	Prairie Creek (USA)	Yes[a]	Yes[b]	bulk Sr-Nd-Hf[b]	
SL7	AV2	Aviat, Rae craton (Canada)	Yes[a]	Yes[b]	bulk Hf[b]	bulk Sr-Nd
SL8	AV6	Aviat, Rae craton (Canada)	Yes[a]	Yes[b]	bulk Hf[b]	bulk Sr-Nd
SL9	KDK/2	Kodomali (India)	Yes[a]	Yes[b]	bulk Sr-Nd-Hf[b]	
SL10	CB	Garledine (India)	Yes[a]	Yes[b]	bulk Sr-Nd-Hf[b]	
SL11	SR/03	Nuapada (India)	Yes[a]	Yes[b]	bulk Hf[b]	bulk Sr-Nd
SL12	SR/05	Nuapada (India)	Yes[a]	Yes[b]	bulk Hf[b]	bulk Sr-Nd
SL13	Behradih	Behradih (India)	Yes[a]	Yes[b]	bulk Sr-Nd-Hf[b]	
SL14	83,211,007	Argyle (Australia)	Yes[a]	Yes[b]	bulk Sr-Nd-Hf[b]	
SL15	RPU/1	Krishna (India)	Yes[a]	Yes[b]	bulk Sr-Nd-Hf[b]	
SL16	TG	Krishna (India)	Yes[a]	Yes[b]	bulk Sr-Nd-Hf[b]	
SL17	83211001B	Argyle (Australia)	Yes[a]	Yes[b]	bulk Sr-Nd-Hf[b]	
SL18	PN-1055	Pionerskaya (Russia)	No	Yes[b]	bulk Sr-Nd-Hf[b]	
SL19	488–510	Lomonoskaya (Russia)	No	Yes[b]	bulk Sr-Nd-Hf[b]	
SL20	SDD3	Seppelt-1 (Australia)	No	Yes[b]	bulk Sr-Nd-Hf[b]	
SL21	S2DD-011	Seppelt-2 (Australia)	No	Yes[b]	bulk Sr-Nd-Hf[b]	
SL22	UBD6	Ashmore (Australia)	No	Yes[b]	bulk Sr-Nd-Hf[b]	
SL23	KC-97-17a	Gaussberg (Antarctica)	No	Yes[b]	bulk Hf[b]	bulk Sr-Nd
SL24	KC-97-23f	Gaussberg (Antarctica)	No	Yes[b]	bulk Hf[b]	bulk Sr-Nd
173/33/K56/10	Newlands	Kaapvaal (South Africa)	Yes[b]	Yes[b]	bulk Nd-Hf[b]	in situ perovskite Sr
NO2-4	Newlands	Kaapvaal (South Africa)	Yes[b]	Yes[b]	bulk Nd-Hf[b]	
173/24/K1/415	Finsch	Kaapvaal (South Africa)	No	No	bulk Nd-Hf[b]	in situ perovskite Sr
173/52/K010/4	Marsfontein M8 (Klipspringer)	Kaapvaal (South Africa)	Yes[b]	Yes[b]	bulk Nd-Hf[b]	in situ perovskite Sr
173/52/K010/4	Marsfontein M8 (Klipspringer)	Kaapvaal (South Africa)	Yes[b]	Yes[b]	bulk Nd-Hf[b]	
173/52/K010/4	Marsfontein M8 (Klipspringer)	Kaapvaal (South Africa)	Yes[b]	Yes[b]	bulk Nd-Hf[b]	
173/33/K106/3	Roberts Victor	Kaapvaal (South Africa)	Yes[b]	Yes[b]	bulk Nd-Hf[b]	in situ perovskite Sr
173/33/K106/3	Roberts Victor	Kaapvaal (South Africa)	Yes[b]	Yes[b]	bulk Nd-Hf[b]	
173/25/K5/9	Sanddrift	Kaapvaal (South Africa)	Yes[b]	Yes[b]	bulk Nd-Hf[b]	in situ perovskite Sr
173/44/K1/17	Star	Kaapvaal (South Africa)	Yes[b]	Yes[b]	bulk Nd-Hf[b]	in situ perovskite Sr
173/26/K15/46	Markt_GR	Kaapvaal (South Africa)	Yes[b]	Yes[b]	bulk Nd-Hf[b]	
173/41/K7/1	Bestershoek	Kaapvaal (South Africa)	Yes[b]	Yes[b]	bulk Nd-Hf[b]	in situ perovskite Sr
AJE718	Sover	Kaapvaal (South Africa)	Yes[b]	Yes[b]	bulk Nd-Hf[b]	
173/33/K102/35	New Elands	Kaapvaal (South Africa)	Yes[b]	Yes[b]	bulk Nd-Hf[b]	in situ perovskite Sr
173/33/K102/44	New Elands	Kaapvaal (South Africa)	Yes[b]	Yes[b]	bulk Nd-Hf[b]	
173/33/K102/44	New Elands	Kaapvaal (South Africa)	Yes[b]	Yes[b]	bulk Nd-Hf[b]	
106.1-PK3/2		West Kimberley (Australia)	Yes[c]	Yes[d]	bulk Sr-Nd-Hf[d]	
106.16-PK12/72		West Kimberley (Australia)	Yes[c]	Yes[d]	bulk Sr-Nd-Hf[d]	
106.17-PK13/1		West Kimberley (Australia)	Yes[c]	Yes[d]	bulk Sr-Nd-Hf[d]	
106.18-PK20/2		West Kimberley (Australia)	Yes[c]	Yes[d]	bulk Sr-Nd-Hf[d]	
107.1-SB35	Smoky Butte	Montana (USA)	Yes[c]	Yes[d]	bulk Sr-Nd-Hf[d]	
107.2-SB45	Smoky Butte	Montana (USA)	Yes[c]	Yes[d]	bulk Sr-Nd-Hf[d]	
107.3-SB59	Smoky Butte	Montana (USA)	Yes[c]	Yes[d]	bulk Sr-Nd-Hf[d]	
107.4-SB66	Smoky Butte	Montana (USA)	Yes[c]	Yes[d]	bulk Sr-Nd-Hf[d]	
107.5-SB70	Smoky Butte	Montana (USA)	No	No	bulk Sr-Nd-Hf[d]	
107.13-BG91-1	Montana	Montana (USA)	Yes[c]	Yes[d]	bulk Sr-Nd-Hf[d]	
107.14-BG92-2	Montana	Montana (USA)	No	No	bulk Sr-Nd-Hf[d]	
107.7-PK5/7		Leucite Hills (USA)	Yes[c]	Yes[d]	bulk Sr-Nd-Hf[d]	
107.8-PK5/9		Leucite Hills (USA)	Yes[c]	Yes[d]	bulk Sr-Nd-Hf[d]	
107.9-PK6/15		Leucite Hills (USA)	Yes[c]	Yes[d]	bulk Sr-Nd-Hf[d]	
107.10-PK9/1		Leucite Hills (USA)	Yes[c]	Yes[d]	bulk Sr-Nd-Hf[d]	
107.11-PL17/19		Leucite Hills (USA)	Yes[c]	Yes[d]	bulk Sr-Nd-Hf[d]	
107.12-PK17/28		Leucite Hills (USA)	No	No	bulk Sr-Nd-Hf[d]	
107.15-MC90-1	Francis	Kamas, Utah (USA)	No	No	bulk Sr-Nd-Hf[d]	
107.6-PK1/4	Prairie Creek	Arkansas (USA)	Yes[c]	Yes[d]	bulk Sr-Nd-Hf[d]	
AF62	HB004 Brockman	Pilbara (Australia)	Yes[a]	Yes[a]	bulk Nd-Hf[a]	
AF63	Brockman 01	Pilbara (Australia)	Yes[a]	Yes[a]	bulk Nd-Hf[a]	

Footnote: For detail analytical data and references refer to Supplementary Tables 1 and 2. Index shows different labs where analysis was done.
[a] – ETH Zürich; [b] – The University of Melbourne; [c] – Geological Survey of Canada; [d] – Durham University.

3.2. XRF analyses

XRF analyses of 19 samples were carried out at ETH Zürich, 15 samples at the University of Melbourne, and 15 samples at the Geological Survey of Canada (GSC) in Ottawa and SGS Lakefield. Analytical procedures at ETH Zürich are as follows. Approximately 1 g of powdered sample was carefully measured and placed into a ceramic crucible. The total loss on ignition (LOI) was determined in an oxygen atmosphere at 500 °C. Following this, the sample was blended in a 1:7 ratio with a lithium tetraborate flux. The mixture was then heated in a platinum crucible at 1000° C to create a circular glass disc for subsequent X-ray fluorescence (XRF) measurements, using a wavelength-dispersive XRF spectrometer (WDS) Axios system from Malvern Panalytical. A variety of certified international and synthetic standards were utilized for primary calibration. At the University of Melbourne, splits of rock powder (~0.6 g) and lithium borate flux (57% tetraborate and 43% metaborate; ~ 4g) were fused at 1050°C in an F-M4 fusion bead casting machine, manufactured by Initiative Scientific Products. The samples were then analyzed on a SPECTRO Xepos energy dispersive X-ray Fluorescence spectrometer. Analytical accuracy was assessed using a variety of internationally certified reference materials (e.g., AGV-1, BCR-2, DNC-1). A similar method was employed at the Geological Survey of Canada (GSC) in Ottawa and SGS Lakefield – details of instrumental techniques are outlined by Tappe et al. (2013). All bulk major element results from this study are compiled in Supplementary Table 2a. Lamproites generally contain a very high proportion of volatiles, thus it is very common to have high LOI (loss of ignition) values for the bulk major analysis. Some of the highest LOI values (up to 24 wt%) in the studied samples reflect hydrous alteration.

3.3. Trace element analyses by ICP-MS

Trace element analyses of 39 samples were carried out at the University of Melbourne, 15 samples at Durham University, and 2 samples at ETH Zürich. At the University of Melbourne, splits (70–90 mg) of the same rock powders employed for XRF analyses were digested on a hotplate, using methods described in Eggins et al. (1997). Solutions for trace element analyses were spiked with ^{6}Li, ^{84}Sr, natural Rh, Re and Bi, and ^{235}U for use as internal standards and run at a dilution factor of ~15000 on an Agilent 7700x quadrupole ICP-MS. The USGS dolerite W-2 was used for calibration (Kamber et al., 2003), while basalt BR and andesite AGV-2 were used to assess data quality and returned results consistent with accepted values (Supplementary Table 2b) (e.g., GeoREM, http://georem.mpch-mainz.gwdg.de). A broadly similar procedure was followed at ETH Zürich where basalt BE-N was employed for calibration and the analyses were undertaken on an Element XR sector field ICP-MS (see details in Fitzpayne et al., 2023). At Durham University, sample preparation and trace element analysis using a Perkin Elmer Sciex Elan 6000 ICPMS follow similar procedures as those described in Ottley et al. (2003). For calibration of instruments internationally recognized rock standards (e.g. W-2, BHVO-1, AGV1) were employed (see details in Ottley et al., 2003). Internal spikes of natural Re and Rh were incorporated to correct matrix suppression and instrumental drift (Ottley et al., 2003). Employing these techniques, the in-house kimberlite standard demonstrated a reproducibility of 2.4% for Lu/Hf ratios and 1.1% for Sm/Nd ratios (Ottley et al., 2003; Nowell et al., 2004). All the trace element results from this study are compiled in Supplementary Table 2a.

3.4. Rb-Sr, Sm-Nd and Lu-Hf isotope analyses by MC-ICP-MS

Whole rock radiogenic isotope compositions for 40 of the 61 samples were measured at the University of Melbourne following similar procedures as in Woodhead et al. (2019) and Dalton et al. (2022) using splits of the same solutions employed for trace element analysis. Weighed solution splits for 24 of the samples were spiked with ^{85}Rb-^{84}Sr, ^{149}Sm-^{150}Nd and ^{176}Lu-^{180}Hf tracers. The remaining 16 samples – mostly of young geological age – were analysed unspiked (see Supplementary Table 2a for an indication of which samples were spiked). Elemental extractions were done using a combination of Eichrom Sr-resin (for Sr), AG50-X8 (200–400) cation exchange resin (Rb) and Eichrom TRU- and LN-resin (Sm, Nd, Lu and Hf). Processing blanks (<0.1 ng Nd, <0.05 ng Hf, <0.05 ng Sm, <0.01 ng Lu) were negligible relative to analyte sizes of 100s to 1000s of nanograms. Isotopic data for the 24 spiked samples were acquired on a Nu Instruments Sapphire multi-collector ICP-MS, with sample uptake via a Glass Expansion PFA nebuliser and a CETAC Aridus desolvating system. The remaining 16 un-spiked samples were analysed on a Nu II Instruments multi-collector ICP-MS. Instrumental mass bias during Sr, Nd and Hf isotopic analyses was corrected by internal normalization to ^{88}Sr/^{86}Sr = 8.37521, ^{146}Nd/^{144}Nd = 0.7219 (or ^{146}Nd/^{144}Nd = 2.0719425 in the case of spiked samples, see Vance and Thirlwall, 2002) and ^{179}Hf/^{177}Hf = 0.7325, respectively, using the exponential law; an on-line iterative spike-stripping/internal normalization procedure was used for the spiked samples. ^{87}Sr/^{86}Sr, ^{143}Nd/^{144}Nd and ^{176}Hf/^{177}Hf of the samples were corrected for the offset between the measured and preferred values of the standards SRM987 = 0.710230, La Jolla Nd = 0.511860 and JMC475 = 0.282160, respectively. External precision (reproducibility, 2sd) is ± 0.000040 (Sr), ± 0.000020 (Nd) and ± 0.000015 (Hf). Instrumental mass bias during Sm isotope dilution analyses was corrected by internal normalization to ^{152}Sm/^{147}Sm =1.78308, after appropriate spike unmixing. Methods for Rb and Lu isotope dilution analyses are based on Waight et al. (2002) and Vervoort et al. (2004), respectively. ^{87}Rb/^{86}Sr, ^{147}Sm/^{144}Nd and ^{176}Lu/^{177}Hf measured by isotope dilution have external precisions of ± 0.5, ± 0.2 and ± 1% (2sd), respectively. The results for Sr-Nd-Hf isotopic ratios for standard materials (e.g., BCR, BHVO-2), including relevant parent/daughter ratios, acquired in this campaign are consistent with reference values (e.g., GeoREM, http://georem.mpch-mainz.gwdg.de) (Supplementary Table 2c). In addition, two analyses were undertaken at ETH Zürich which follow the same procedure as for the unspiked samples measured at the University of Melbourne (see details in Fitzpayne et al., 2023).

Isotopic data for the remaining 19 samples (all of young geological age (≤ 162 Ma), thus they were analysed unspiked; Supplementary Table 2a) were acquired at Durham University. Whole rock digestions were carried out in 15mL Savillex Teflon beakers using approximately 100 mg of sample powder. All dry-downs were conducted using infrared lamps in a HEPA filtered clean air environment to minimise the possibility of fall-in blank during the evaporation. The technique for separating Sr, Nd, and Hf in samples employed the two anion exchange columns described by Dowall et al. (2003). Once collected from the ion-exchange columns, the Hf, Sr, and Nd fractions were evaporated to dryness and then dissolved in 1 mL of 3% HNO_3 solution. The sample solutions were introduced into the plasma using an ESI PFA-50 microflow nebulizer and a dual cyclonic Scott double pass (CSDP) quartz spray chamber. For samples with lower concentrations, a Cetac Aridus desolvating nebulizer was used for sample introduction. All isotope measurements were done using a ThermoFinnigan Neptune PIMMS (*aka* MC-ICP-MS) instrument at Durham University. All sample data are normalized relative to the following accepted or recommended standard values, Hf: ^{176}Hf/^{177}Hf ratio of 0.28216 for JMC475 (Blichert-Toft et al., 1997); Nd: ^{143}Nd/^{144}Nd ratios of 0.511110 for J&M (equivalent to the accepted La Jolla value) (Royse et al., 1998); Sr: ^{87}Sr/^{86}Sr ratio of 0.71025 for NBS 987 (Thirlwall, 1991). The reproducibility of the ^{176}Hf/^{177}Hf, ^{143}Nd/^{144}Nd and ^{87}Sr/^{86}Sr ratios for appropriate standard solutions (JMC 475, J&M Nd, and NBS 987 respectively) of the Durham Neptune is in all cases better than 0.04 ng/g and consistent with the accepted values and are reported in Dowall et al. (2003).

A total of 36 (out of 61) samples were analyzed for bulk-rock Sr isotopic compositions, with published bulk-rock Sr isotope data available for 7 of the samples (Murphy et al., 2002; Chalapathi Rao et al., 2016, Das et al., 2018; Sarkar et al., 2018; Supplementary Tables 1 and

2). Sixteen of the remaining samples are from the Kaapvaal craton, with in-situ Sr isotope data from perovskites available for 8 of these samples, as reported by Woodhead et al. (2009) (Supplementary Tables 1 and 2). Two samples from Brockman Creek (Pilbara) were not analyzed for Sr because their very old age and alteration suggest a likely strong perturbation of the Rb-Sr system. Nd isotope analyses were conducted on 54 samples, whereas all 61 samples underwent Hf isotopic analyses (out of these, we present the first Hf analyses for 53 localities; Supplementary Table 2). The Nd isotopic compositions for the remaining 7 samples were sourced from the literature (Murphy et al., 2002; Chalapthi Rao et al., 2013; Das et al., 2018; Sarkar et al., 2018). Age-corrected εNd and εHf values are calculated relative to modern CHUR composition with $^{147}Sm/^{144}Nd = 0.1960$, $^{143}Nd/^{144}Nd = 0.512630$, $^{176}Lu/^{177}Hf = 0.0336$ and $^{176}Hf/^{177}Hf = 0.282785$ (Bouvier et al., 2008). The εSr values are calculated as age-corrected variation from the evolution of an assumed "Bulk Silicate Earth" present-day value of $^{87}Sr/^{86}Sr = 0.7045$, and using a time-integrated $^{87}Rb/^{86}Sr$ of 0.0827. Decay constants are: ^{87}Rb $1.397x10^{-11}$/yr (Villa et al., 2015); ^{147}Sm $6.54x10^{-12}$/yr (Begeman et al., 2001); ^{176}Lu $1.865x10^{-11}$/yr (Scherer et al., 2001). All isotopic data produced in this study are compiled in Supplementary Table 2a.

4. Results

4.1. Major element compositions

The studied samples exhibit a wide range in major element compositions: 30.3 to 53.3 wt% SiO_2, 2.9 to 13.5 wt% CaO, 5.7 to 28.2 wt% MgO, 1.3 to 5.6 wt% TiO_2, and up to 9.7 wt% K_2O. These data are plotted in Fig. 2, together with lamproites from our newly compiled global database (Supplementary Table 1). The major element compositions obtained for fresh lamproites in this study generally align with previously published data for the same localities or lamproites in the corresponding clusters, with minor exceptions (Fig. 2). For example, the Cenozoic West Kimberley lamproite samples analysed in this study display elevated levels of SiO_2 (up to 50 wt% in total), Al_2O_3, and K_2O, but lower MgO contents compared to values from the literature (Fig. 2), probably due to presence of minor crustal material in the former. Furthermore, major element covariation plots highlight the overall diversity in global cratonic lamproite compositions (e.g., ~20–57 wt% SiO_2; ~2–35 wt% CaO; up to ~10 wt% TiO_2; up to ~13 wt% K_2O), while also revealing a weak inverse relationship between CaO and SiO_2 and a moderate positive correlation between SiO_2 and Al_2O_3 (Fig. 2).

The Kaapvaal lamproites exhibit some of the broadest variations in SiO_2 and CaO contents (ranging from 20 to 48 wt% and 2 to 35 wt%, respectively) among the examined provinces (Fig. 2c). Yet, all the lamproites from different provinces within this craton were classified together based on their similar age. The Wajrakarur lamproites show lower concentrations of K_2O (up to 2.7 wt%) compared to Kaapvaal lamproites (up to 6.72 wt%), whereas their SiO_2 and CaO contents overlap with the compositions observed in the Kaapvaal lamproites (Fig. 2c). The Smoky Butte, Leucite Hills, Gaussberg (Antarctica), and certain Cenozoic West Kimberley lamproites exhibit higher SiO_2, Al_2O_3, and K_2O contents than cratonic lamproites elsewhere (Fig. 2a, 2d, 2f). In addition, the Smoky Butte, Luangwa valley (Zambia) lamproites, and certain Cenozoic West Kimberley samples display the highest TiO_2 contents (Fig. 2).

4.2. Trace element compositions

Absolute trace element concentrations for the samples analysed in this study show large variations both within and between individual lamproite clusters (Fig. 3). For example, across the entire sample suite, Ba and La concentrations vary from 118 ppm to 16,771 ppm and 21 ppm to 630 ppm, respectively (Fig. 3). Importantly, the samples investigated in this study closely align with previously reported trace element data from the same localities or lamproite clusters, as also noted above for major element concentrations (see Supplementary Table 1b). It is also notable that, for the global lamproites, elements that are considered to be relatively immobile in hydrous fluids, such as La, Nb, Th and Gd display well correlated inter-elemental arrays whereas the fluid mobile elements (e.g., Ba, Rb) exhibit more 'dispersed' data patterns when plotted against an immobile element such as La (Fig. 3). It is important to note that lamproites from some localities (e.g., Kaapvaal lamproites) show positive correlations between La, Nb, Th, and Pb (Fig. 3a, 3b, 3c), indicating magmatic fractionation or, more likely, variable dilution by entrained xenocrystic olivine. Cratonic lamproites undergo very limited fractionation during ascent as they do not stall in deep magmatic chambers, else they would lose most of their mantle cargo.

Similar to existing data, primitive mantle (PM)-normalized trace element plots of the samples analysed in this study (Fig. 4) show enrichment in large ion lithophile elements (LILE) and LREEs compared to HREE, and negative K, Sr and P anomalies (Fig. 4; Supplementary Fig. S1). One exception is represented by the Kaapvaal lamproites, where large variations in the HREEs concentrations are observed (Fig. 4b). Notably, lamproites from West Kimberley (Cenozoic), Leucite Hills, Francis, Prairie Creek (Arkansas), Antarctica, and Cuddapah exhibit the highest levels of LREE enrichment, whereas those from Arkhangelsk and a subset of the Kaapvaal lamproites are less enriched (Fig. 4). The Smoky Butte lamproites are characterized by unique, more subdued LILE enrichment patterns, with HREE contents closely resembling those of the Cenozoic West Kimberley and Leucite Hills lamproites (Fig. 4c). The Ashmore-Seppelt lamproite samples exhibit the largest negative P anomalies (Fig. 4a). The Brockman Creek (Pilbara) lamproites exhibit the largest negative K anomalies, and the Arkhangelsk and a subset of Kaapvaal lamproite samples show distinctive negative Zr-Hf anomalies (Fig. 4b, 4c).

4.3. Sr-Nd-Hf isotope compositions of the examined samples

Initial $^{87}Sr/^{86}Sr$ values for the current samples vary significantly across different lamproite provinces (0.703698 to 0.719069), although $^{87}Sr/^{86}Sr_{(i)}$ values show a more restricted range within individual clusters (Supplementary Table 2). For example, the Prairie Creek (Arkansas) lamproites (n = 3) exhibit initial $^{87}Sr/^{86}Sr$ values ranging from 0.706592 ± 0.000013 to 0.706901 ± 0.000017, with $\varepsilon Sr_{(i)}$ values ranging from 31.5 to 35.9. Conversely, the Cenozoic West Kimberley lamproites exhibit an extreme range (0.714032 ± 0.000010 to 0.719069 ± 0.000008; n = 4), extending to the most radiogenic $^{87}Sr/^{86}Sr_{(i)}$ values recorded for the entire sample suite (Fig. 5a). With the exception of the Bunder lamproite samples, all other samples examined in this study have similar Sr isotopic compositions relative to published values for lamproites in the same locality or cluster (Fig. 5).

Similar to the Sr isotopic compositions, initial $^{143}Nd/^{144}Nd$ values vary widely from 0.509816 ± 0.000020 (Brockman Creek) to 0.512222 ± 0.000009 (Kodomali, Bastar craton) (Supplementary Table 2a); however, initial $^{176}Hf/^{177}Hf$ values display a more restricted range of 0.281225 ± 0.000005 (Brockman Creek) to 0.282598 ± 0.000011 (Pionerskaya, Arkhangelsk) (Supplementary Table 2a). The $\varepsilon Nd_{(i)}$ and $\varepsilon Hf_{(i)}$ values of the samples studied range from 1.1 to –23.7 and 2.4 to −34, respectively, and are again comparable to previously reported values for lamproites from a given area (Fig. 5). Notably, we present the first Nd-Hf isotopic data for lamproites from Brockman Creek (n = 2; $\varepsilon Nd_{(i)} = -4.5$ to −4.6; $\varepsilon Hf_{(i)} = -10$ to −10.1) and Ashmore-Seppelt (n = 3; $\varepsilon Nd_{(i)}$ = 0.7 to 1.1; $\varepsilon Hf_{(i)} = -1.7$ to 1.9; Fig. 5). In the analysed samples, the initial εNd and εHf values exhibit significantly more variation in some areas compared to others. For example, the Kaapvaal lamproites (12 samples) show a wide range in $\varepsilon Nd_{(i)}$ (−5 to −10.7) and $\varepsilon Hf_{(i)}$ (−3.9 to 15.3) values (Fig. 5). In contrast, the Cenozoic West Kimberley, Smoky Butte lamproites (5 samples) display a much narrower range in $\varepsilon Nd_{(i)}$ (−13.5 to −15.4; –23.1 to –23.7, respectively) and $\varepsilon Hf_{(i)}$ (−20.9 to 25.3; –32 to −34, respectively) values (Fig. 5). The Nd-

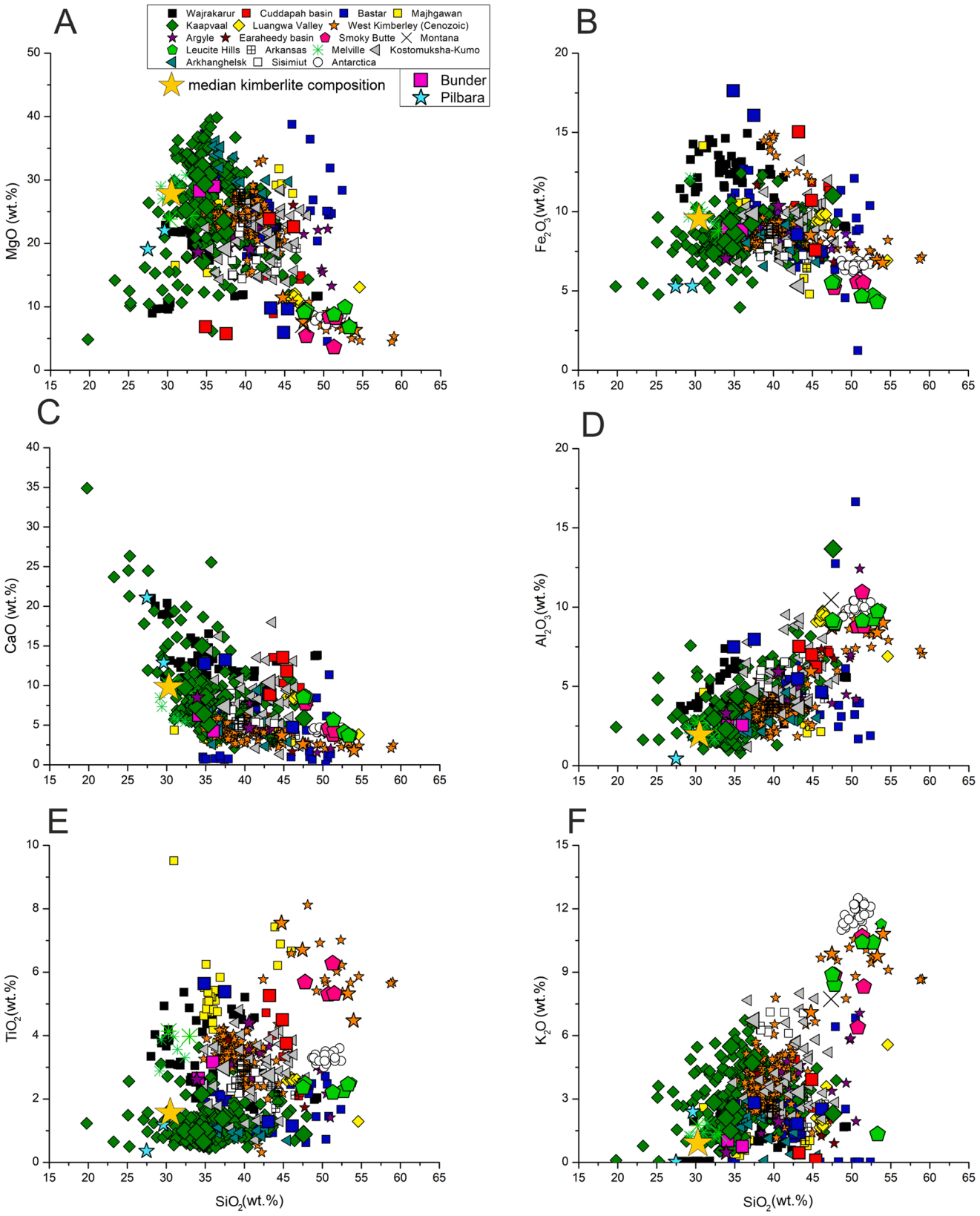

Fig. 2. Covariation plots of MgO (a), Fe_2O_3 (b), CaO (c), TiO_2 (d), Al_2O_3 (e), and K_2O (f) against SiO_2 for the global lamproite dataset. Larger data points are from this study (Supplementary Table 2). For major element compilation refer to Supplementary Table 1b. Median kimberlite composition (yellow star) is from Giuliani et al. (2024).

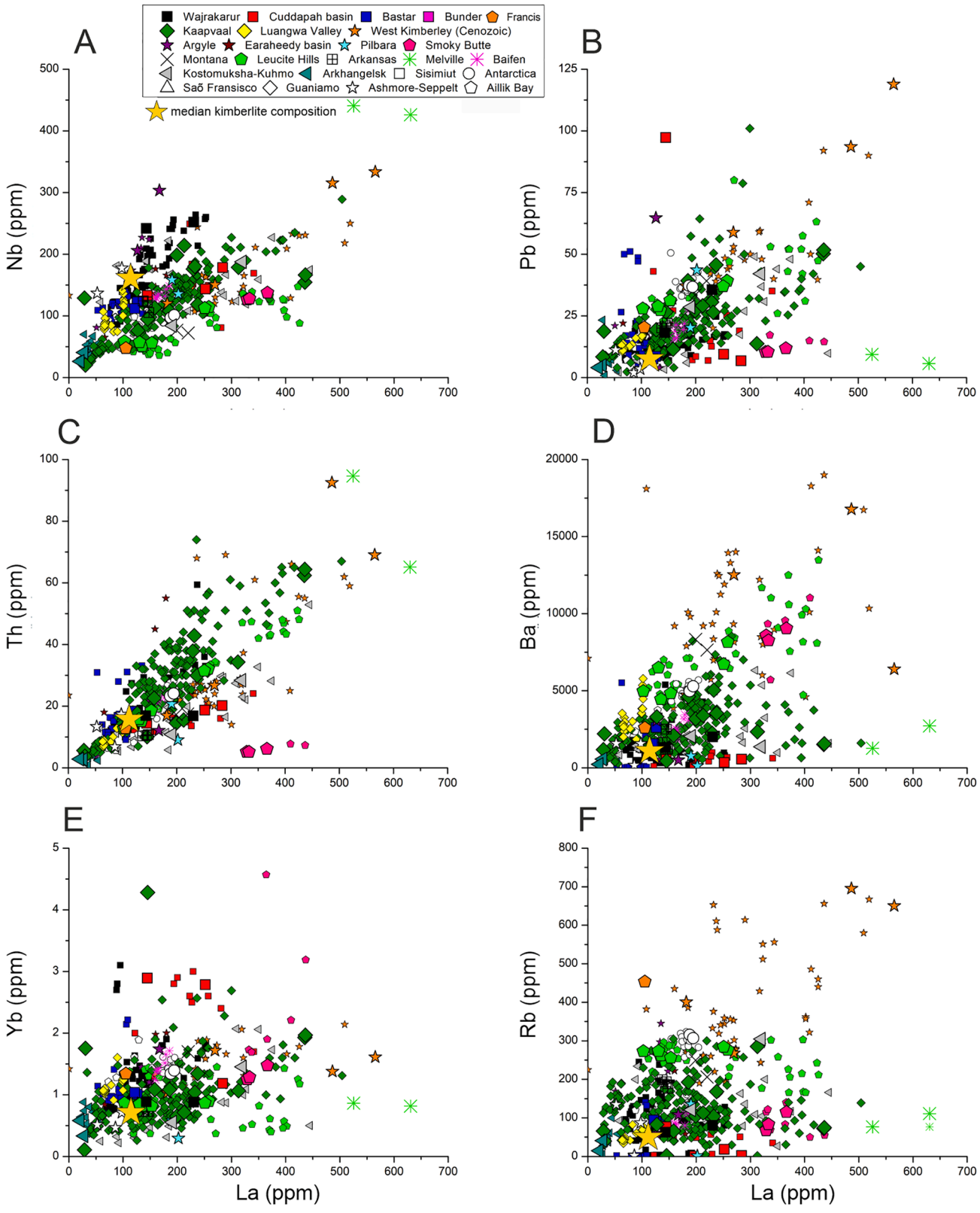

Fig. 3. Trace element covariation plots for the global lamproite database: La vs a) Nb; b) Pb; c) Th; d) Ba; e) Yb; f) Rb. For the trace element compilation see Supplementary Table 1b. Larger symbols denote data from this study. The median kimberlite composition is from Giuliani et al. (2024).

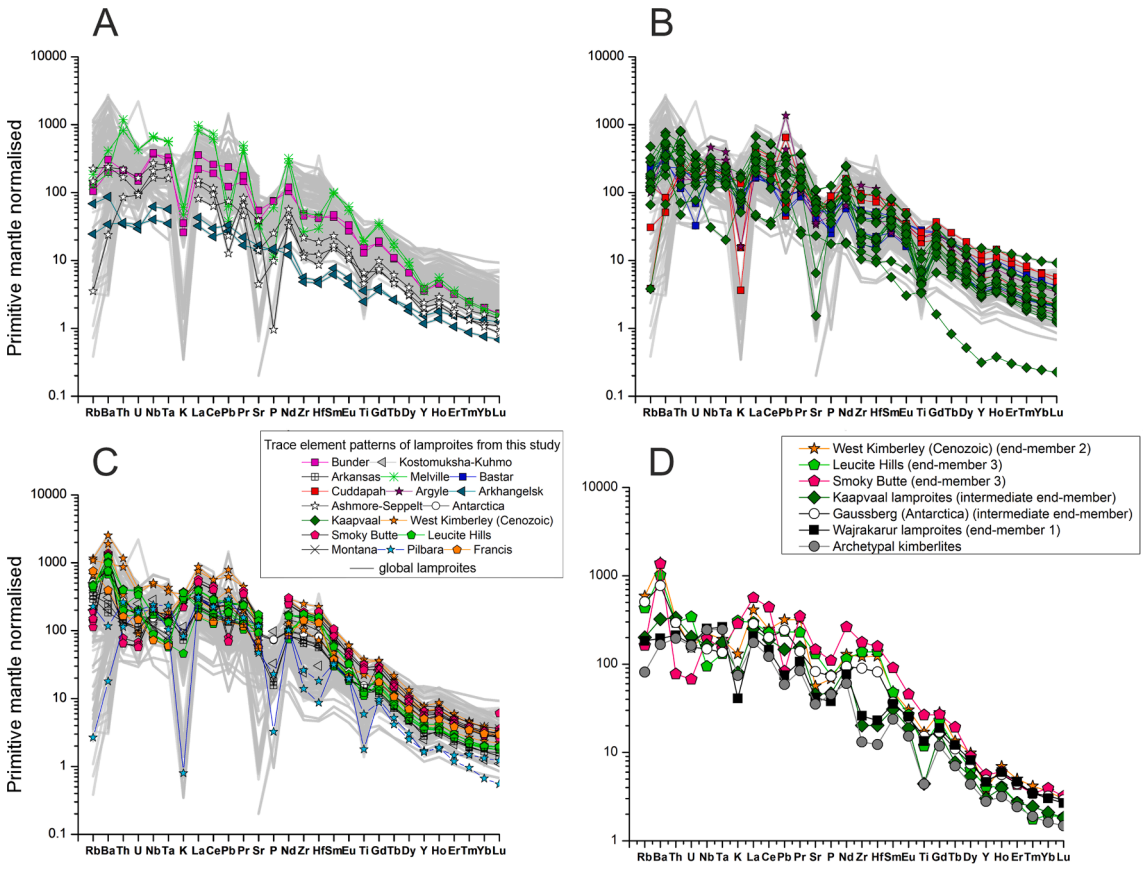

Fig. 4. Primitive mantle-normalized bulk-rock trace element patterns of lamproites from this study (a, b, c) and globally. Dark Grey bands are published global lamproite data, whereas, the rest of the colored symbols are lamproites from this study. (d) Primitive mantle-normalised bulk-rock trace element patterns of archetypal kimberlites and representative end-member lamproites including lamproites from Wajrakarur (end-member 1); Cenozoic West Kimberley (end-member 2); Leucite Hills and Smoky Butte (end-member 3); Kaapvaal and Gaussberg (isotopically intermediate lamproites). All trends represent median compositions for each lamproite cluster. Primitive mantle values are from McDonough and Sun (1995).

Hf isotopic compositions of all the examined samples are similar to other cratonic lamproites worldwide (Supplementary Table 1a), but are less radiogenic compared to most of the archetypal kimberlites worldwide (e.g., Woodhead et al., 2019; Giuliani et al., 2021, 2024).

4.4. Variations in global lamproite isotopic data

Sr-Nd-Hf isotopic data for global lamproites, including new data derived from this study are plotted in $\varepsilon Sr_{(i)}$-$\varepsilon Nd_{(i)}$, $\varepsilon Sr_{(i)}$-$\varepsilon Hf_{(i)}$, and $\varepsilon Nd_{(i)}$-$\varepsilon Hf_{(i)}$ space along with data for global ocean island basalts (OIBs) and archetypal kimberlites (representative of purely asthenospheric melts) (Fig. 5). As crustal contamination or alteration of lamproite samples can adversely affect Rb/Sr ratios and measured $^{87}Sr/^{86}Sr$ results, we do not consider data which plots more than 50 $\varepsilon Sr_{(i)}$ units away from those of other coeval samples from the same area. A first-order observation from the global compilation is that the majority of lamproites are highly geochemically-enriched compared to global OIBs or archetypal kimberlites (Fig. 5).

Within the global Sr-Nd-Hf data, three distinct isotopic end-members can be discerned. The first end-member (hereafter referred to as "end-member 1"; dashed black circle region in Fig. 5a, b) includes lamproites from Wajrakarur, Bunder, Melville, Arkhangelsk, Guaniamo and Ashmore-Seppelt. These lamproites have more geochemically-depleted Sr-Nd-Hf compositions which overlap with both OIB and kimberlite compositions and plot close to the BSE (Bulk-Silicate Earth) composition (Fig. 5). End-member 2 corresponds to the array defined by the Cenozoic West Kimberley lamproites, which exhibit elevated $\varepsilon Sr_{(i)}$ values (ranging from 84 to 242), but a smaller range in $\varepsilon Nd_{(i)}$ (−7.4 to −18.6) and $\varepsilon Hf_{(i)}$ (−20.9 to −25.3) values (Red arrow in Fig. 5a, b). Notably, the extreme $\varepsilon Sr_{(i)}$ nature of these lamproites is also observed in the most extreme, enriched mantle (EM-II) compositions shown by Samoan OIBs (εSr up to 225) (e.g., Jackson et al., 2007; Adams et al., 2021), however, the Cenozoic West Kimberley lamproites have less radiogenic Nd-Hf isotopic compositions (Fig. 5a, b). The third isotopic end-member (referred to as "end-member 3"; Magenta arrow in Fig. 5a, b) is represented by lamproites from Leucite Hills, Smoky Butte and Sisimiut (Greenland), with values that extend from BSE to highly negative $\varepsilon Nd_{(i)}$-$\varepsilon Hf_{(i)}$ values (−7 to −28.7 and −8.1 to −34, respectively) and moderately positive $\varepsilon Sr_{(i)}$ values (<30). The end-member 3 classification excludes two Sisimiut data points of $\varepsilon Sr_{(i)}$ 77 and 86.4 and one Leucite Hills data points of $\varepsilon Sr_{(i)}$ 46.7, which may have disturbed Sr isotope values as they plot at similar Nd but more radiogenic Sr values than the other samples from the same province. Beyond these three end-members, the remaining lamproites have 'intermediate' isotopic compositions (dashed green region in Fig. 5a, b) and fall in between the BSE-like depleted lamproites (end-member 1) and the extreme groups of lamproites (end-member 2 and 3) (Fig. 5a, b). Notably, the Gaussberg lamproite samples (shown as 'Antarctica' in Fig. 5), and Francis from Utah (USA), have the most enriched isotopic compositions ($\varepsilon Nd_{(i)}$ and $\varepsilon Hf_{(i)}$ values of −12 to −14.9 and −21.5 to −21.7, respectively) within the 'intermediate' lamproite suite (Fig. 5a, b). Details of each end-member, highlighting the localities and their geochemical affinities/signatures, are summarized in Table 2.

When assessing the global compilation as a whole, the lamproite isotopic compositions (Fig. 5a, b), 'fan out' in $\varepsilon Sr_{(i)}$-$\varepsilon Nd_{(i)}$ and $\varepsilon Sr_{(i)}$-$\varepsilon Hf_{(i)}$ spaces, from the most geochemically-depleted lamproite compositional end-member 1 (close to BSE values) to the direction of end-

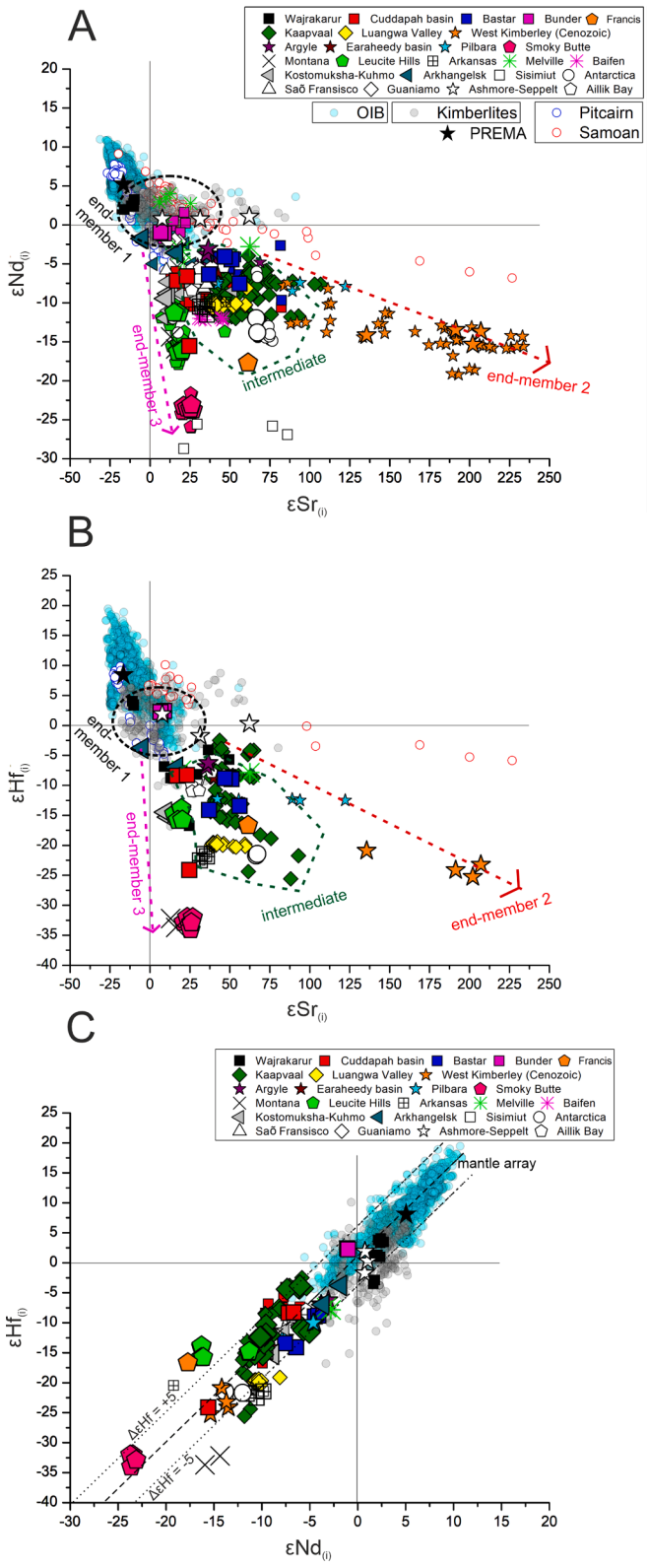

Fig. 5. Bulk Sr-Nd-Hf isotope covariation plots for global cratonic lamproites (Supplementary Table 1a). Larger data points refer to samples from this study (Supplementary Table 2). Note different end-member lamproite groups are represented by dashed arrows or dashed areas (see also Table 2). Archetypal kimberlites and OIBs from the compilations of Giuliani et al. (2021) and Stracke et al. (2022) respectively, are shown for comparison. The kimberlite-based PREMA (PREvalent MAntle) component is from Giuliani et al. (2021). The Nd-Hf mantle array (black dashed line in (c)) is taken from Vervoort et al. (2011).

member 2 and 3 compositions or at intermediate compositions (e.g., Kaapvaal, Gaussberg). This pattern is also observed for global OIBs and carbonatites, albeit with less extreme isotopic values (e.g. Stracke et al., 2022; Yaxley et al., 2022). It is interesting to note in Sr-Nd isotope space that, similar to the EM end-members identified in OIBs, the two geochemically-enriched lamproite end-members, 2 and 3, do not appear to show mixing relationships with each other, but exclusively with the geochemically-depleted end-member 1 (e.g. Hart et al., 1992; also see discussion). Furthermore, in the $\varepsilon Nd_{(i)}$-$\varepsilon Hf_{(i)}$ plot (Fig. 5c), all lamproite compositions are roughly aligned along the mantle array, extending through OIBs and kimberlites to more extreme compositions – exceptions being positive $\Delta\varepsilon Hf$ values (measured as the vertical displacement from the mantle array using the equation: $\Delta\varepsilon Hf = \varepsilon Hf - (1.55 \times \varepsilon Nd + 1.21)$; Vervoort et al., 2011) for Leucite Hills (+ Francis) (1.5 to 10.2) and negative for Bear Gulch (Montana) lamproites (−10.2 to −11.2) (Fig. 5c). The almost complete lack of deviations from the Nd-Hf mantle array differs from the frequent negative $\Delta\varepsilon Hf$ values observed in kimberlites (Nowell et al., 2004; Tappe et al., 2020; Dalton et al., 2022; Sarkar et al., 2023; Giuliani et al., 2024).

4.5. *Covariation of radiogenic isotopes and major-trace element compositions*

The initial εNd isotope compositions of global lamproites are plotted against their major element concentrations in Fig. 6. Global lamproites display broad inverse relationships between initial εNd values and SiO_2 and K_2O contents (Fig. 6a, 6d). Specifically, lamproites from Smoky Butte, Leucite Hills, Bear Gulch (Montana), Antarctica, and West Kimberley (Cenozoic), which are characterized by the most geochemically enriched isotopic compositions and the lowest initial εNd values (i.e., end-members 2 and 3; Fig. 5), generally have the highest SiO_2 and K_2O contents (up to 57 wt% and 12.2 wt%, respectively) (Fig. 6d). In contrast, lamproites that isotopically resemble the Bulk Silicate Earth (BSE) (end-member 1) and have higher initial εNd values, such as those from Wajrakarur, Bunder, and Melville, tend to have lower K_2O (~0.5 to 2.5 wt%) and SiO_2 (~30 to 38 wt%) contents (Fig. 6c, 6d). Lamproites from Smoky Butte and Cenozoic West Kimberley also exhibit the highest TiO_2 content (up to 10.5 wt%). Similar to the major elements, lamproites from these localities and Antarctica tend to have higher Th/Nb (up to 0.55), Ba/Th (up to 1175), and Zr/Nd (up to 27) ratios, along with lower Ce/Pb (up to 17.2) and Nb/La (up to 0.7) ratios when compared to other lamproites, and the depleted MORB mantle or DMM (Th/Nb = 0.05; Ba/Th = 71; Zr/Nd = 8.7; Ce/Pb = 30.6; Nb/La = 0.77) (Workman and

Table 2
Summary table for each end-member lamproite group.

End-member	Features	Samples/Locations
End-member 1 (dotted black region in Fig. 5a, b)	geochemically-depleted Sr-Nd-Hf compositions, overlap with both OIB and kimberlite compositions and plot close to the BSE (Bulk-Silicate Earth) composition	Wajrakarur, Bunder, Melville, Arkhangelsk, Guaniamo, Ashmore-Seppelt
End-member 2 (Red array in Fig. 5a, b)	elevated $\varepsilon Sr_{(i)}$ values (ranging from 84 to 242), but a smaller range in $\varepsilon Nd_{(i)}$ (−7 to −19) and $\varepsilon Hf_{(i)}$ (−21 to −25) values	Cenozoic West Kimberley
End-member 3 (Magenta array in Fig. 5a, b)	extend from BSE to highly negative $\varepsilon Nd_{(i)}$-$\varepsilon Hf_{(i)}$ values (−7 to −29 and −8 to −34, respectively) and moderately positive $\varepsilon Sr_{(i)}$ values (<30)	Leucite Hills, Smoky Butte, Sisimiut, Montana, Kostomuksha-Kuhmo
Intermediate (dotted green region in Fig. 5a, b)	fall in between the BSE-like depleted lamproites (end-member 1) and the extreme groups of lamproites (end-member 2 and 3)	Kaapvaal, Luangwa valley, Bastar, Pilbara, Cuddapah basin, Aillik Bay, São Francisco, Argyle, Earaheedy basin, Baifen, Francis, Arkansas, Gaussberg

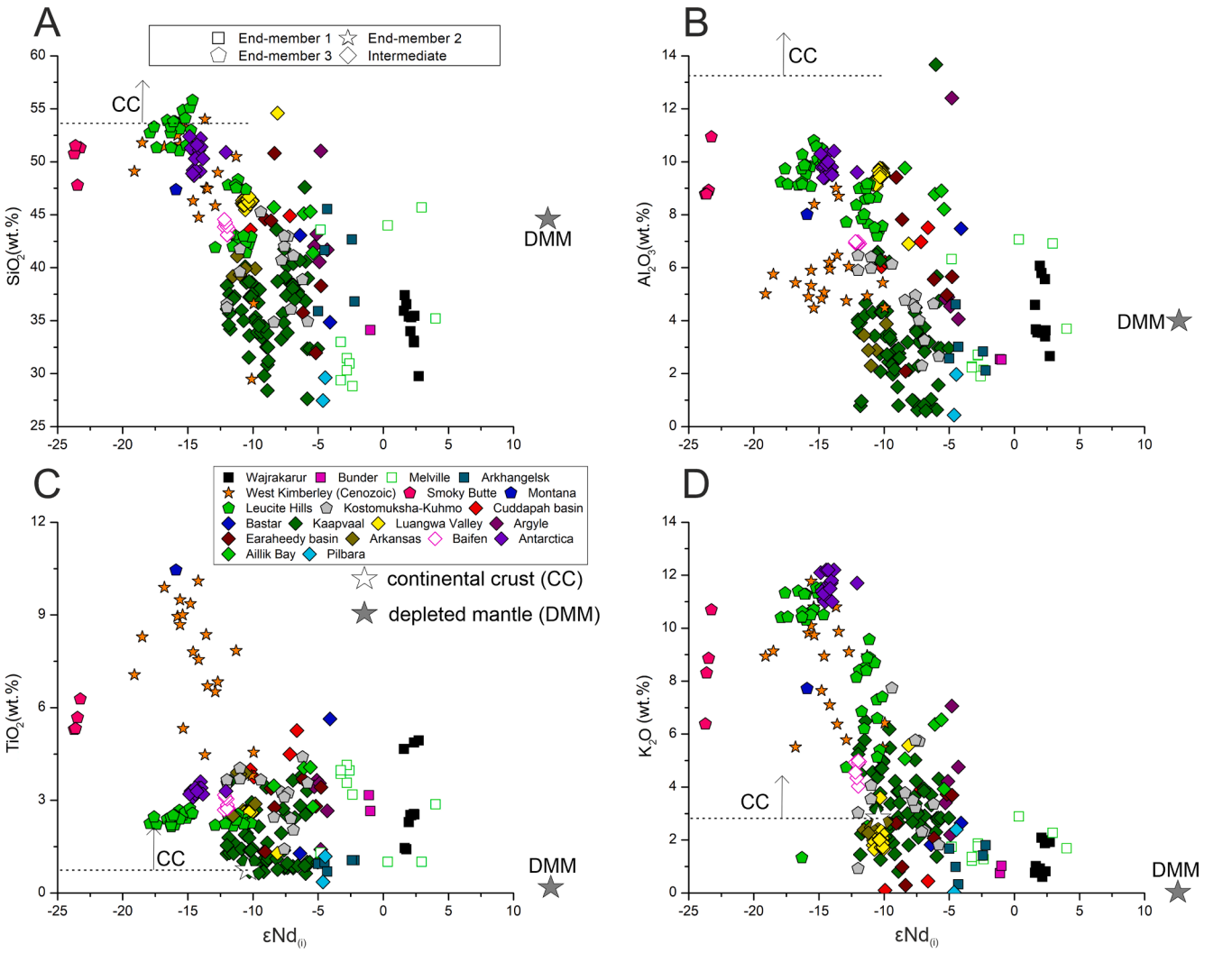

Fig. 6. Covariation plots of SiO_2 (a), TiO_2 (b), Al_2O_3 (c), and K_2O (d) versus age-corrected initial Nd isotope compositions of global lamproites. The dotted black line shows the range of Nd isotopic composition of continental crust. Major element compositions of depleted MORB mantle (DMM) and continental crust (CC) are from Workman and Hart (2005) and Rudnick and Gao (2014) respectively. Isotopic composition of depleted MORB mantle (DMM) is from Konter et al. (2008). Isotopic compositional range of continental crust (CC) is from McCulloch and Wasserburg (1978), Gaschnig et al. (2022) and Desem et al. (2025). For the compilation of bulk major elements and isotopic compositions see Supplementary Table 1.

Hart, 2005). These lamproites have lower Th/Nb ratio but higher Ba/Th, Zr/Nd, Ce/Pb and Nb/La ratios compared to continental crust (Th/Nb = 0.88; Ba/Th = 60; Zr/Nd = 7.1; Ce/Pb = 3.7; Nb/La = 0.38) (Rudnick and Gao, 2014) (Fig. 7). Notably, the Smoky Butte lamproites display the highest Ba/Th ratio (up to 2729) (Fig. 7c). Finally, geochemically-depleted lamproites (i.e. end-member 1 lamproites with highest initial εNd values), such as those from Wajrakarur, exhibit lower Th/Nb (up to 0.14) and Zr/Nd (up to 4.9) ratios, but higher Nb/La (up to 1.5) ratios than the geochemically-enriched lamproites of end-members 2 (e.g. Cenozoic West Kimberley lamproites) and 3 (e.g. Leucite Hills lamproites) (Fig. 7).

5. Discussion

5.1. The least geochemically enriched lamproites (end-member 1)

Lamproites from Wajrakarur, Bunder (both in India), and Melville (Canada), as well as most of the lamproites in the Arkhangelsk (Russia), Guaniamo (Venezuela) and Ashmore-Seppelt (Australia) areas, overlap with both OIBs and kimberlites and plot close to BSE values in $\varepsilon Sr_{(i)}$-$\varepsilon Nd_{(i)}$-$\varepsilon Hf_{(i)}$ compositional space (Fig. 5). This suggests that these lamproites might share similar source(s) with OIBs and archetypal kimberlites. Archetypal kimberlites worldwide are believed to originate from either mantle plumes or asthenospheric mantle sources (Smith, 1983; Chalapathi Rao, 2004; Nowell et al., 2004; Tappe et al., 2013, 2018; Pearson et al., 2019; Woodhead et al., 2019; Giuliani et al., 2023), and more specifically to frequently tap a common mantle component akin to PREMA (PREvalent MAntle; Zindler and Hart, 1986) (see Giuliani et al., 2021, 2024). The overlap between lamproites with isotopic characteristics similar to BSE (end-member 1) and archetypal kimberlites plus OIBs suggests that the convective mantle may be the dominant source component for this sub-set of lamproites (Fig. 5). Supporting evidence for this model comes from the suggestion made by several authors (Chalapathi Rao et al., 2016; Das et al., 2018; Shaikh et al., 2018; Sarkar et al., 2021, 2022; Xu et al., 2021) that the Wajrakarur lamproites and kimberlites (India) may have originated from similar convective mantle sources, with compositional differences caused by interaction with different SCLM materials (e.g., phlogopite-rich material in the case of K-enriched lamproites). Previous studies clearly indicate that the compositional variations of these lamproites cannot be attributed to a single mantle source but instead require a combination of at least two components: convective and lithospheric. Consequently, we

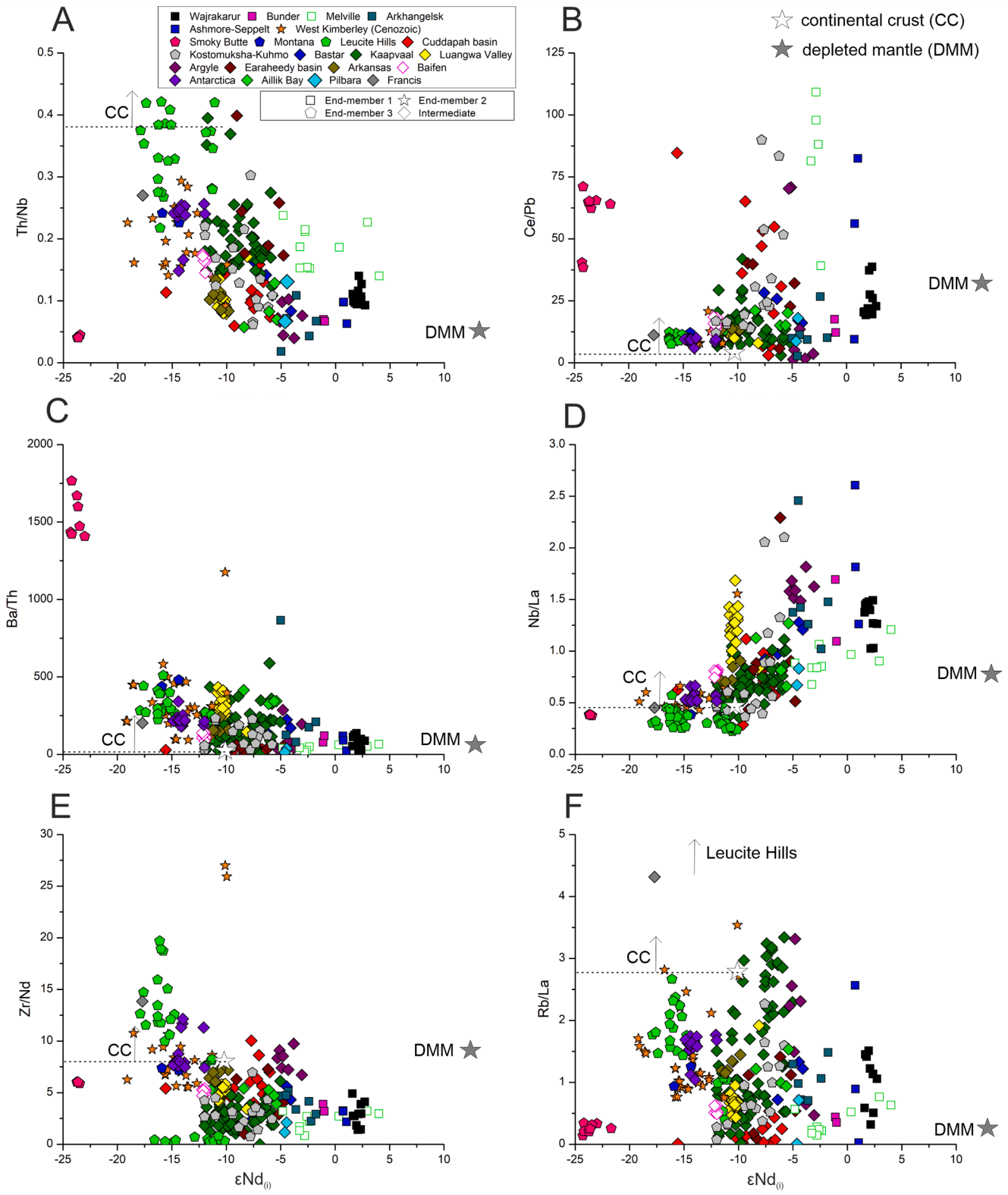

Fig. 7. Covariation plots of trace element ratios versus age-corrected initial Nd isotope compositions of global lamproites. The dotted black line shows the range of Nd isotopic composition of continental crust. Trace element compositions of depleted MORB mantle (DMM) and continental crust (CC) are from Workman and Hart (2005) and Rudnick and Gao (2014) respectively. Isotopic composition of depleted MORB mantle (DMM) is from Konter et al. (2008). Isotopic compositional range of continental crust (CC) is from McCulloch and Wasserburg (1978), Gaschnig et al. (2022) and Desem et al. (2025). For the compilation of trace elements and isotope compositions see Supplementary Table 1.

present simple mixing models below to approximate the isotopic variations of these lamproites based on different source components.

To further explore the above hypothesis, we performed binary mixing models (Table 3; Fig. 8) with our starting proto-lamproite component based on an age-corrected PREMA-like melt (Jackson and Jellinek, 2013; Giuliani et al., 2021), as a suitable approximation of an asthenospheric convective component. This melt is then mixed with an enriched lithospheric mantle component represented by MARID (Mica-Amphibole-Rutile-Ilmenite-Diopside) xenoliths, a proxy for extremely metasomatised, enriched regions in the SCLM from the Kaapvaal craton (Fitzpayne et al., 2019) (i.e. mixing of melt and assimilated solid components). The MARID xenoliths reported in Fitzpayne et al (2019) are predominantly hosted in Kaapvaal kimberlites, including those employed to define the MARID endmember, and only occasionally in lamproites. There is ample evidence that lamproites could be derived from MARID-bearing mantle or at least their genesis has a link to MARID rocks (e.g., Giuliani et al., 2015). Thus, we have used MARID in our mixing models as a proxy for K-rich metasomes or as extreme enriched lithospheric endmember. All the mixing parameters, compositions of different components used in the mixing models, and mixing equations are presented in Table 3 and Supplementary Table 3. The Sr, Nd, and Hf concentrations of the PREMA-derived melt are based on the mean composition of low-degree OIB melts (Stracke et al., 2022) instead of kimberlite melts. This is justified because, although OIBs and kimberlites share a similar PREMA source (e.g. Giuliani et al., 2021), OIBs have lower CO_2 content compared to kimberlites and are therefore more suitable proxies to model the genesis of low-CO_2 lamproites (Supplementary Table 1b). Isotopic compositions of the mixing components, i.e., PREMA and MARID, are age-corrected to approximate their composition at the time of eruption for the respective lamproites (similarly, this has been done for each end-member lamproite; see below). The binary mixing models at 500, 800, and 1200 Ma (Fig. 8c, 8d, 8e, 8f) demonstrate that, in the majority of cases, the corresponding age-corrected PREMA/asthenospheric component plots close to the lamproites defining end-member 1 (e.g. Wajrakarur, Melville, Bunder, Arkhangelsk, Ashmore-Seppelt). A minor contribution (up to ~30%) from MARID (as illustrated in Fig. 8c, 8e) appears to be essential to fully account for the Sr-Nd isotopic variations observed in this subset of lamproites. However, in Nd-Hf isotopic space (Fig. 8d, 8f), a higher amount of MARID (up to 90%) is required for some of these lamproites (e.g., Arkhangelsk), which probably hints to variability in the mineralogy and isotopic composition of the MARID component. In general, the combination of a dominant asthenospheric component (70–90% PREMA-like melt) with minor input from geochemically-enriched lithospheric components (10–30% MARID) is consistent with the overall major and trace element compositions of these lamproites (Figs. 2, 4d, 6, 7). For example, the Wajrakarur lamproites, being the most geochemically depleted samples in $\varepsilon Sr_{(i)}$-$\varepsilon Nd_{(i)}$-$\varepsilon Hf_{(i)}$ compositional space (Fig. 5), have comparatively low SiO_2 and K_2O contents (Fig. 6a, 6d) and exhibit only marginally higher LILE and REE contents compared to kimberlites (Fig. 4d), but comparable Th/Nb, Ce/Pb, and Ba/Th ratios to kimberlites (Giuliani et al., 2024) and DMM (Fig. 7). Furthermore, the Wajrakarur lamproites show characteristic negative Zr-Hf anomalies in trace element patterns, similar to kimberlites (Fig. 4d), a key feature for melt derived from carbonated peridotites most likely in the asthenospheric mantle. These geochemical characteristics are also evident in the mineralogy of these lamproites, with Wajrakarur lamproites exhibiting a relatively higher concentration of carbonate phases in their groundmass compared to other lamproite groups.

In summary, isotopic compositions that align with both global kimberlites and OIBs, coupled with the overall resemblances in major and trace elements chemistry to kimberlites, and results from binary mixing models, suggest that the BSE-like lamproites of end-member 1 likely originate from a predominant convective-mantle component (e.g. PREMA), with a minor contribution from assimilated metasomatised mica-bearing lithospheric material (Fig. 8c, 8d, 8e, 8f). It is important to highlight that we modelled our mixing calculations to align with the eruption ages of the end-member 1 lamproites (and similarly for other end-members, as discussed below), employing a backward modelling approach rather than forward modelling. Forward modelling, which involves calculating mantle separation ages and predicting the resulting εSr-εNd-εHf values at the time of lamproite eruption, was not used because the high Rb/Sr ratio of MARID (e.g., Fitzpayne et al., 2018) would produce unrealistically elevated Sr isotope values that do not correspond to any known lamproite end member or mixing scenario within a few hundred million years. For instance, Supplementary Fig. S2 illustrates that MARID evolution from an initial PREMA like isotopic compositions would yield εSr values ranging from ~230 to ~1700 over 200–1500 Myr of growth, far exceeding the εSr value of 230 observed in the most Sr-rich lamproite. This is inconsistent with the much longer ageing of the metasomatic component suggested by Nd and Hf isotopes and thus, strongly supports the backward modelling approach presented in this study.

Table 3
Details of binary mixing models.

For Fig. 8	
Depleted component	solid PREMA mantle PREMA derived melt
Enriched component	MARID xenolith Subducted slab (80 % EMORB + 20 % GLOSS II) Subducted slab (0 % EMORB + 100 % GLOSS II)
For Fig. 9	
Depleted component	PREMA derived melt
Theoretical Enriched component	A = 90 % Narssaq Peridotite + 10 % MARID (with least radiogenic Sr) B = 90 % Narssaq Peridotite + 10 % MARID (with most radiogenic Sr) C = 90 % Narssaq Peridotite + 10 % Subducted slab (80 % EMORB + 20 % GLOSS II) D = 90 % Narssaq Peridotite + 10 % Subducted slab (0 % EMORB + 100 % GLOSS II)
Mixing equation	$R_{mix} = \frac{R_i \times C_i \times f + R_{ii} \times C_{ii} \times (1-f)}{C_i \times f + C_{ii} \times (1-f)}$ R = isotope ratio; C = element concentration; f = mixing proportion in fraction i = depleted component; ii = enriched component

Footnote: Isotopic ratios and elemental concentrations for each component and respective references are mentioned in Supplementary Table 3. Narssaq peridotite composition is from Van de Löcht et al. (2020). PREMA: PREvalent Mantle (Giuliani et al., 2021); MARID: mica-amphibole-rutile-ilmenite-diopside (Fitzpayne et al., 2019); EMORB: enriched mid-oceanic ridge basalt (Gale et al., 2013); GLOSS: global subducting sediments (Plank, 2014).

5.2. The end-member 2 lamproites (Cenozoic West Kimberley)

The Cenozoic lamproites from West Kimberley (end-member 2) display extremely radiogenic Sr isotope compositions, mirroring the characteristics of OIBs with EM II signatures (i.e. Samoa) in $\varepsilon Sr_{(i)}$-$\varepsilon Nd_{(i)}$ and $\varepsilon Sr_{(i)}$-$\varepsilon Hf_{(i)}$ plots (Fig. 5). However, Cenozoic West Kimberley lamproites display a steeper slope compared to EM-II OIBs in $\varepsilon Sr_{(i)}$-$\varepsilon Nd_{(i)}$ and $\varepsilon Sr_{(i)}$-$\varepsilon Hf_{(i)}$ plots (Fig. 5a and 5b) including less radiogenic $\varepsilon Nd_{(i)}$ and $\varepsilon Hf_{(i)}$ values, suggesting that these lamproites may not directly derive from the same source as EM II OIBs from Samoa (e.g., Jackson et al., 2007; Adams et al., 2021). The OIBs with EM II signatures are generally considered to contain contributions from subducted continental crust or related sedimentary materials (Zindler and Hart, 1986; Weaver, 1991; Chauvel et al., 1992; Jackson et al., 2007; Jackson and Dasgupta, 2008), emphasizing the possible contribution of continental crust to the source(s) of the Cenozoic West Kimberley lamproites. A crustal contribution to the lamproite source aligns with inverse relations between SiO_2, K_2O and isotopic compositions (Fig. 6) and elevated Th/Nb, Ba/Th, Zr/Nd ratios, and lower Ce/Pb and Nb/La ratios observed in

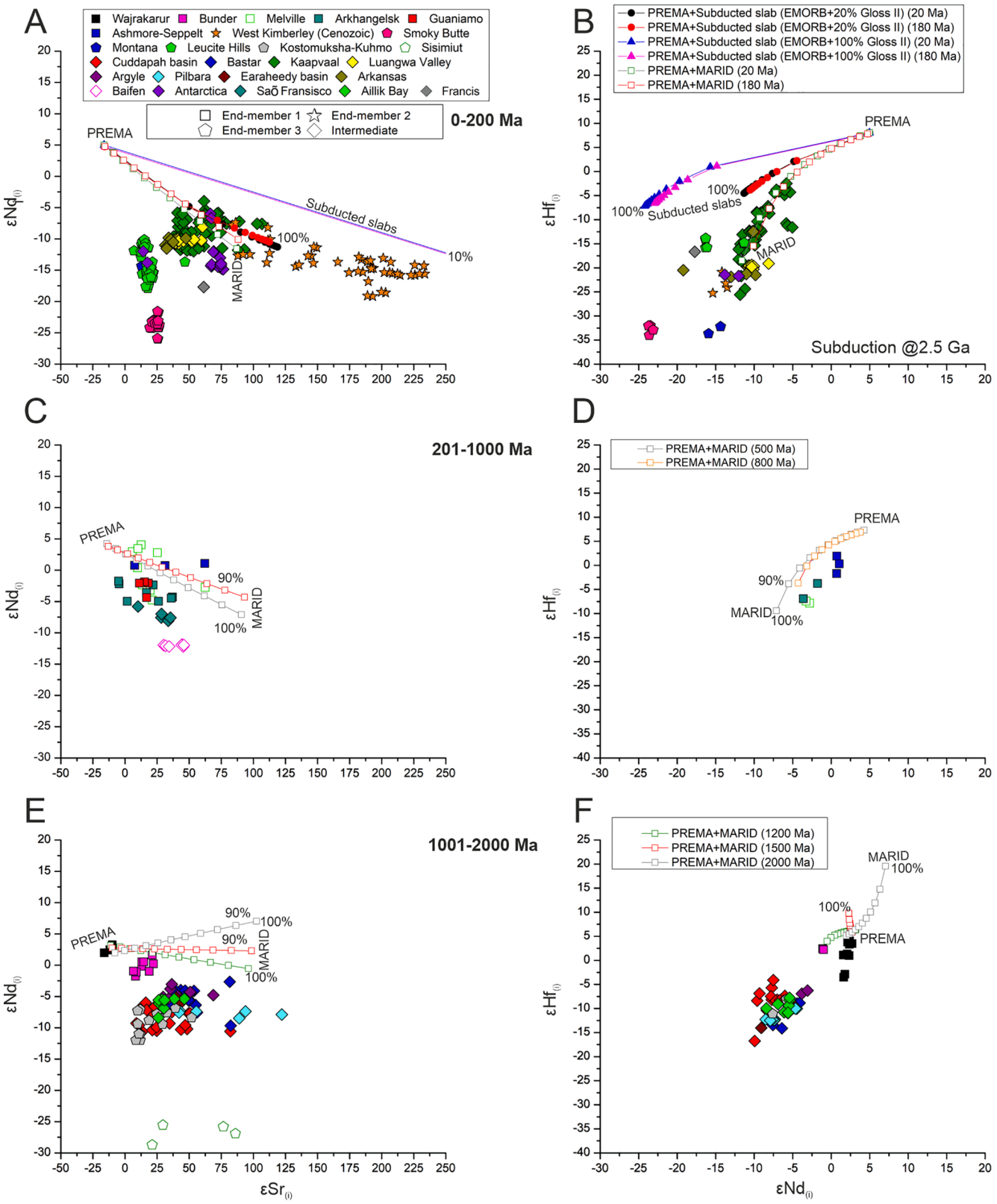

Fig. 8. Bivariate plots of $\varepsilon Sr_{(i)}$ vs $\varepsilon Nd_{(i)}$ (a, c, e) and $\varepsilon Hf_{(i)}$ vs $\varepsilon Nd_{(i)}$ (b, d, f) for worldwide cratonic lamproites showing binary mixing models between different natural end-member components. The whole lamproite dataset is divided into three age groups to better match the binary mixing models – 0–200 Ma, 201–1000 Ma, and 1001–2000 Ma. Models are run at 20, 180, 500, 800, 1200, 1500, and 2000 Ma ages and 10% increments are shown on the mixing lines using an empty symbol. The convective-mantle PREMA component (note both PREMA-like mantle (solid component) and PREMA-derived melt are used in (a) and (b), whereas in (c), (d), (e), and (f) only PREMA-derived melt is used; see text for details) is from Giuliani et al. (2021) and MARID is from Fitzpayne et al. (2019). Subducted material is composed of EMORB (Gale et al., 2013) and GLOSS II (Plank (2014) mixed in variable proportions. Compositions of subducted component adjusted to account for subduction-induced modification following Stracke et al. (2003). See Table 3 and Supplementary Table 3 for detailed model parameters.

these lamproites (Fig. 7), although the extreme Ti enrichment (TiO_2 = 3.8–10.1 wt%; Fig. 6c; Supplementary Fig. S3) is at odds with crustal assimilation or simple addition of a subducted crustal component. Alternatively, Jaques et al. (1984) suggested derivation of these lamproites from low degree partial melting of formerly depleted upper mantle peridotite that was strongly enriched in K, and other incompatible elements including LILEs, LREEs and HFSEs via mantle metasomatism with introduction of phlogopite, rutile and ilmenite (also see Fig. 4d and Supplementary Table 1b).

To investigate the genesis of end-member 2 lamproite(s) exemplified by the Cenozoic West Kimberley lamproites, we explore the possibility that subducted slab components are blended into a PREMA-like asthenospheric mantle source (i.e. solid–solid mixing) or that melts derived from PREMA mixed with enriched phlogopite-bearing lithospheric mantle (i.e. mixing of liquid and assimilated solid components) (Table 3). Mixing between two components in the genesis of these lamproites is justified by the spread in Sr-Nd isotope compositions, extending from moderately to extremely geochemically-enriched compositions ($\varepsilon Sr_{(i)}$ values ranging from 84 to 242; Fig. 5 and Fig. 8a, 8b). The lithospheric mantle component is represented by MARID rocks (Fitzpayne et al., 2019) and the subducted component comprises 0 to 80% EMORB (enriched mid-oceanic ridge basalt; Gale et al., 2013) and 20% to 100% GLOSS II (global subducted sediments; Plank, 2014). Modification of the subducted component(s) through dehydration or partial melting during subduction was determined using the calculations of Stracke et al. (2003) (also see Kogiso et al., 1997; Johnson and Plank, 2000). All the model parameters are listed in Table 3 and Supplementary Table 3. The model combining a melt from a PREMA source and assimilated MARID wall rocks at 20 Ma age fails to explain the isotopic variations of Cenozoic West Kimberley lamproites (Fig. 8a, 8b), whereas a model combining a PREMA source with subducted slabs, likely in the asthenospheric mantle region, at 20 Ma age closely matches the array of Cenozoic West Kimberley lamproite compositions in the $\varepsilon Sr_{(i)}$-$\varepsilon Nd_{(i)}$ plot (Fig. 8a). However, the resultant trend deviates in the $\varepsilon Nd_{(i)}$-$\varepsilon Hf_{(i)}$ plot (Fig. 8b), highlighting the inadequacy of existing natural mantle compositions (as utilized for mixing models) in the literature to explain the isotopic variations of these lamproites. Therefore, additional theoretical modelling appears to be required to account for the isotopic variations of these lamproites (Fig. 9a, 9b).

For the theoretical modelling, the isotopic composition of PREMA is again used for the depleted endmember represented by a melt sourced from the convective mantle (Table 3). For the theoretically enriched components, a combination (90:10) of different lithologies is employed (Table 3). The first component is a mica-bearing peridotite xenolith from the Narssaq ultramafic body, West Greenland (Van de Löcht et al., 2020), with unradiogenic Nd-Hf isotopic values. The second is the same subducted slab component as used above. It is worth noting that the theoretical blend of peridotite (90%) and subducted slab (10%) proposed here could have originated within the lithospheric mantle if a subducted slab component or a slab-derived fluid had previously interacted with lithospheric peridotite, resulting in the formation of the enriched assemblage (see enriched components in Fig. 9). The high P-T experimental works of Wunder and Melzer (2003), Meltzer and Kessel (2022, 2023) and Gao et al. (2023) have shown that metasomatised peridotites containing phlogopite, K-richterite, and minor ilmenite and rutile can indeed be generated by the interaction of high-density H_2O-rich fluids released by subducted slabs with peridotites. It is also important to highlight that our choice of the enriched component is such that the Sr isotopic variation is predominantly governed by the Rb/Sr ratio of the subducted slab component and the age of subduction (e.g., 2.5 Ga used in these models), whereas the variation in Nd-Hf isotopes is controlled by the peridotite component due to its higher Nd and Hf contents. In Fig. 10a and 10b, the mixing model of PREMA-derived melt + enriched component D (where the subducted slab includes only GLOSS II) at 20 Ma age reflects the most extreme geological scenario, where no EMORB component is considered. This model extends beyond the most extreme isotopic variations of the Cenozoic West Kimberley lamproites and could theoretically account for the range in $\varepsilon Sr_{(i)}$ values (Fig. 9a, 9b). However, this or similar theoretical models (i.e. with slightly different proportions of EMORB and GLOSS-II) predict 90% of assimilated material would be required, which contradicts basic energetic and thermal constraints on the amount of wall rock material that can be assimilated in a melt. Thus, as previously suggested by Sarkar et al. (2022) to explain the K-Al enrichment and olivine composition of cratonic lamproites, it is more likely that mixing is mediated by the "selective assimilation" of metasomatic components instead of bulk peridotite assimilation. In this process the PREMA-derived melt could preferentially incorporate incompatible elements (including Sr, Nd, Hf) from incongruent melting of metasomatic minerals such as mica and amphibole residing in the metasomatised lithospheric at the time of ascending melt-lithosphere interaction/assimilation (e.g., components C and D in Fig. 9). Therefore, the high levels of assimilation (up to 90%) required by the mixing models reflect the amount of incompatible trace elements supplied by the geochemically-enriched lithospheric components rather than the amount of assimilated (solid) material. For example, formation of peritectic olivine during phlogopite break-down (Sarkar et al., 2022) drastically limits the amount of solid material that is assimilated in the melt, whereas the bulk of K, Rb and (mostly radiogenic) Sr residing in phlogopite are released into the melt. A similar model was recently put forward by Jaques (2024) who suggested that interaction of small-volume asthenospheric melts with subduction-modified metasomatised lithospheric mantle could have generated the geochemical enrichment observed in the Cenozoic West Kimberley lamproites.

The occurrence of phlogopite and, potentially, K-richterite, ilmenite and rutile in the assimilated metasomatic assemblage could account for the highly radiogenic Sr isotope composition of the lamproite source as well as the elevated SiO_2, K_2O and TiO_2 (Fig. 6), and incompatible trace element contents (Figs. 4, 7), which are characteristic of these lamproite melts (Fig. 6; Jaques et al., 1984; Fitzpayne et al., 2018; Foley et al., 2022; Foley and Ezad, 2024). The required enriched metasomatised lithospheric assemblage for these end-member 2 lamproites likely originates from the previous addition of subducted-slab fluids to the lithospheric mantle, suggested by elevated Ba/Th and Rb/La, and low Ce/Pb and Nb/La compared to DMM (Fig. 7). It could be argued that the isotopically extreme compositions of Cenozoic West Kimberley lamproites (e.g., very low initial εNd values) along with their elevated SiO_2, K_2O contents, and Th/Nb ratios (Figs. 6, 7) suggest crustal assimilation. However, the high Ti content of these lamproites (Fig. 6) contradicts the idea of simple crustal assimilation. In addition, we have calculated the proportion of continental crust required to account for the isotopic compositions of the studied lamproites (see details in Supplementary Fig. S4). The models indicate that achieving the observed Nd isotopic variations would require 50% to 90% crustal assimilation. Such a high degree of crustal assimilation is unlikely, as most of the studied samples are relatively fresh and do not exhibit pervasive crustal contamination to support such an extreme scenario. Finally, we shall note that cratonic lamproites form small volcanic/sub-volcanic complexes and are not associated with magmatic chambers which, combined with the very high concentrations of incompatible trace elements, limit the amount of potential crustal contamination in these magmas. Therefore, we propose that the crustal signature observed in these lamproites originates from phlogopite, K-richterite, ilmenite and rutile bearing metasomatised lithospheric mantle (as depicted from theoretical mixing models; Fig. 9), modified by a subduction-derived component, rather than from 'typical' crustal assimilation at shallower depths. The presence of ilmenite and rutile along with phlogopite and K-richterite in the metasomatized SCLM for these lamproites aligns with their elevated SiO_2, K_2O, and TiO_2 contents (see also inverse correlations between Nd isotope and SiO_2, K_2O, and TiO_2 contents in Figs. 6 and 7), as well as the elevated modal abundances of phlogopite (often Ti-bearing), leucite, K-richterite and accessory phases like ilmenite and Ti-rich minerals such as priderite in

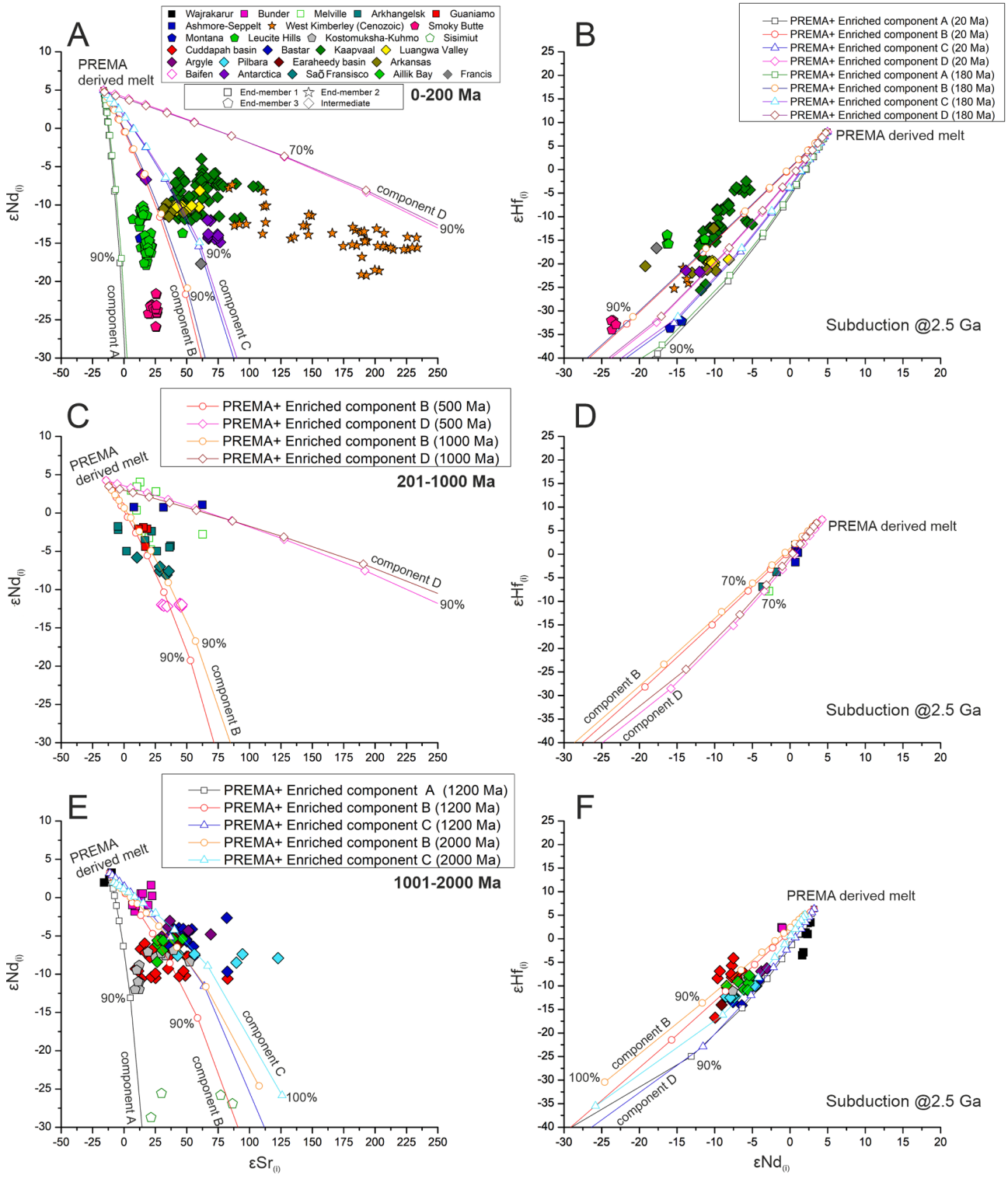

Fig. 9. Bivariate plots of $\varepsilon Sr_{(i)}$ vs $\varepsilon Nd_{(i)}$ (a, c, e) and $\varepsilon Hf_{(i)}$ vs $\varepsilon Nd_{(i)}$ (b, d, f) for the cratonic lamproites worldwide showing binary mixing relationship between a PREMA-derived melt (Giuliani et al., 2021) and different theoretical enriched components (see index; Table 3 and Supplementary Table 3). Note that the whole lamproite dataset is divided into three age groups to better represent the binary mixing models, 0–200 Ma, 201–1000 Ma, and 1001–2000 Ma. Models are run at 20, 180, 500, 1000, 1200, and 2000 Ma ages and 10% increments are shown on the mixing lines using an empty symbol. The theoretical enriched components are as follows: A = 90 % Peridotite + 10 % MARID (least radiogenic Sr); B = 90 % Peridotite + 10 % MARID (most radiogenic Sr); C = 90 % Peridotite + 10 % Subducted slab (80 % EMORB + 20 % GLOSS II); D = 90 % Peridotite + 10 % Subducted slab (0 % EMORB + 100 % GLOSS II). The peridotite composition is from Van de Löcht et al. (2020) and MARID compositions are from Fitzpayne et al. (2019). Subducted material is composed of EMORB (Gale et al., 2013) and GLOSS II of Plank (2014), adjusted to account for subduction-induced modification following Stracke et al. (2003). See Table 3 and Supplementary Table 3 for model parameters.

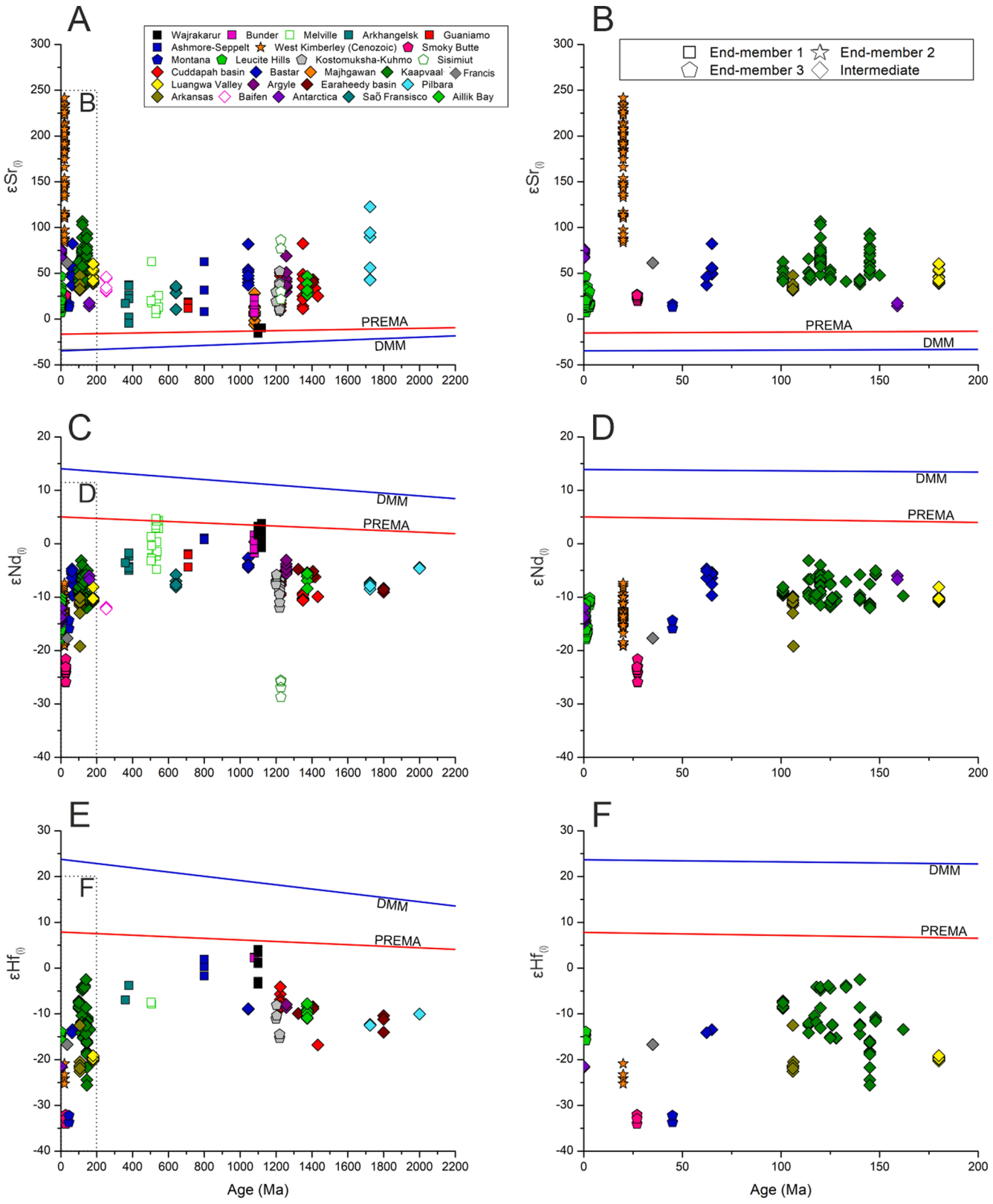

Fig. 10. Temporal distribution of (a), (b) initial Sr, (c), (d) Nd, and (e), (f) Hf isotopic compositions of global cratonic lamproites. For the data compilation see Supplementary Table 1a. (b), (d) and (f) represent "zoomed in" views into the last 200 Ma. Isotopic evolution lines of depleted MORB mantle (DMM) and PREvalent Mantle (PREMA) are plotted from Konter et al. (2008) and Giuliani et al. (2021) respectively.

the groundmass (Jaques et al., 1984). Finally, the highly radiogenic Sr and unradiogenic Nd isotopic composition suggests mantle enrichment beneath the West Kimberley region extends back to at least 1000 Ma, based on previous models of radiogenic ingrowth (e.g. Jaques et al., 1984; Foley and Ezad, 2024). In our binary mixing calculations, we utilized a subduction age of 2500 Ma, which provides the long-term residence required for the source(s) to achieve sufficient ingrowth of radiogenic Sr from a mica-rich peridotite with elevated Rb/Sr. Contribution by an ancient metasomatic component stored in the lithosphere is further supported by the distinctive Pb isotope compositions of these lamproites, characterized by low $^{206}Pb/^{204}Pb$ ratios and high $^{207}Pb/^{204}Pb$ and $^{208}Pb/^{204}Pb$ ratios (McCulloch et al., 1983; Nelson et al., 1986).

In summary, based on the binary mixing models, we propose that the interaction of a convective-mantle melt, with a long-lived, predominantly phlogopite-K-richterite-ilmenite-rutile-bearing lithospheric component, derived from ancient subduction-induced metasomatism, yields the isotopic trends observed in the Cenozoic West Kimberley lamproites (end-member 2). A similar geochemically-enriched component may have also contributed to other lamproites with similar although less extreme geochemical signature (e.g., Gaussberg, Kaapvaal; Figs. 5, 9).

5.3. The end-member 3 lamproites (Leucite Hills and Smoky Butte)

The Smoky Butte lamproites (United States) extend towards the most negative $\varepsilon Nd_{(i)}$ and $\varepsilon Hf_{(i)}$ (as low as −26 and −35, respectively) values of the global lamproite dataset (Fig. 5). This remarkable enrichment may derive from phlogopite-bearing metasomatized lithosphere, as suggested by the elevated SiO_2, Al_2O_3, K_2O and TiO_2 contents of Smoky Butte lamproites, or from subduction-related LILE-rich fluids, as indicated by high Ba contents alongside low Th, Nb, and Zr concentrations in these lamproites including extreme Ba/Th fractionation (Figs. 2, 6, 7; Supplementary Table 1b). However, their elevated Ce/Pb values (Fig. 7b) are at odds with a connection to subduction-related fluids. Lamproites from Leucite Hills and Bear Gulch (Montana) are also characterized by extremely negative $\varepsilon Nd_{(i)}$ and $\varepsilon Hf_{(i)}$ values and exhibit some geochemical features akin to Smoky Butte, including elevated K_2O and SiO_2 contents and high Ba contents, but elevated Th/Nb, Zr/Nd plus low Ce/Pb values (Figs. 2, 6, 7; Supplementary Table 1b). Previous studies have proposed that extremely negative $\varepsilon Nd_{(i)}$-$\varepsilon Hf_{(i)}$ (as observed in end-member 3; Fig. 5) in lamproites either originate from anciently enriched metasomatized phlogopite-bearing lithospheric mantle (e.g., Fraser et al., 1985) or metasomatism linked to ancient, subducted siliciclastic sediments (Mitchell and Bergman 1991; Davies et al. 2006; Mirnejad and Bell 2006; Tappe et al. 2007; Sun et al. 2014, 2021; Xiang et al. 2020). Thus, the sources of the end-member 3 lamproites remain an open question.

To address this issue, we first attempt to define which natural components in the Earth's mantle have isotopic composition approaching end-member 3 lamproites from Smoky Butte, as an example (Table 3; Fig. 5). No published MARID, i.e. the most extreme metasomatised rocks in the SCLM, or subducted components extend to the extremely negative $\varepsilon Nd_{(i)}$ and $\varepsilon Hf_{(i)}$ compositions at low to moderate $\varepsilon Sr_{(i)}$ values (mostly up to 30) of these lamproites (Fig. 8). Not surprisingly, the identification of this enigmatic enriched component has long represented a challenge (e.g. Fraser et al., 1985; Sun et al., 2021). Recently, Foley and Ezad (2024) have proposed that clinopyroxene or K-richterite could be a source for lamproites with these compositions; however, their isotopic compositions do not explain such extreme Sr-Nd-Hf isotopic values. Therefore, we must utilize theoretical components to model (Table 3) the observed isotopic, as well as major and trace element compositions in these lamproites.

Similar to the previous section, we construct two enriched components which consist of a 90:10 combination of SCLM peridotite (taken from Van de Löcht et al., 2020) with either MARID with the least radiogenic and the most radiogenic Sr compositions (Fitzpayne et al., 2019) or subducted material (80% EMORB + 20% of GLOSS II), respectively (Enriched component A, B and C respectively; Fig. 9; see Table 3 and Supplementary Table 3). These theoretical components represent metasomatised phlogopite-rich peridotites and MARID-veined peridotites, respectively, at lithospheric depth. It is important to note that in both cases, Sr isotopic variations are controlled by Rb/Sr ratio and ages of either MARID or subducted slab component, which are also enriched in Sr. The peridotite component again dominates the Nd and Hf budgets and, hence, their isotopic signatures. These theoretical components achieve and extend beyond the geochemically-enriched isotopic signatures of end-member 3 lamproites either when MARID metasomatism is assumed to have occurred at 20 Ma or for subduction at 2500 Ma (Fig. 9a, d).

The compositional array extending from lamproites with BSE-like isotopic values to Smoky Butte (i.e. the most geochemically-enriched lamproites defining end-member 3), including the spread observed in the Leucite Hills lamproites, can be representative of the variations in the composition of the metasomatised lithospheric mantle source. Alternatively, as explored below, these compositional variations reflect mixing between a convective-mantle melt, for example with PREMA-like or more geochemically-enriched composition, and some of the theoretical metasomatised lithospheric mantle components defined above. The three mixing models at 20 Ma between a melt from a PREMA-like source and components A, B and C all produce $\varepsilon Sr_{(i)}$-$\varepsilon Nd_{(i)}$ and $\varepsilon Nd_{(i)}$-$\varepsilon Hf_{(i)}$ arrays that approximate the isotopic compositions shown by Leucite Hills and Smoky Butte lamproites (Fig. 9a, b). However, in the case of older lamproites with end-member 3 signature (e.g., Sisimiut and Kostomuksha-Kuhmo-Lentira at ~1.2 Ga), only the combination of peridotite and MARID with the least radiogenic Sr isotopes (i.e. Enriched component A) provide a good fit (Fig. 9e, f). Thus, we speculate that assimilation of ~80–95% of Sr-Nd-Hf (and other incompatible trace elements) from an anciently metasomatised phlogopite-rich SCLM component by an ascending melt derived from the convective mantle is a viable process to generate some of the variations observed across the end-member 3 lamproites. Similar to what was described above for end-member 2 lamproites, this scenario requires selective rather than bulk assimilation of geochemically-enriched material (see discussion in the previous section). Further, the occurrence of mica-bearing peridotites in minettes from the Highwood Mountains and Eagle Butte, exhibiting highly negative Nd ($\varepsilon Nd_{(i)}$ up to −39) and less radiogenic Sr isotopic compositions ($^{87}Sr/^{86}Sr_{(i)}$ up to 0.71) (Carlson and Irving, 1994), provides support to our model where metasomatised lithosphere with extremely unradiogenic Nd isotopes likely participated in the genesis of end-member 3 lamproites (e.g., Leucite Hills, Smoky Butte) from the Montana/Wyoming province.

It is also possible that a subducted component might be an additional local factor in some cases, as observed in a few lamproites from Leucite Hills and Sisimiut that have more radiogenic $\varepsilon Sr_{(i)}$ (up to 80) (Fig. 9a, e). However, in these cases we suspect perturbation of Sr isotopes by alteration rather than peculiar components with anomalously high $^{87}Sr/^{86}Sr$ due to the indistinguishable Nd isotopic compositions of these high-$^{87}Sr/^{86}Sr$ samples compared to others from the same locality. Regardless, input by subducted material most likely in the form of slab-derived fluids/melts that metasomatised the lithospheric mantle, which is subsequently assimilated, is consistent with high Ba/Th, Th/Nb and low Nb/La values (Fig. 7) and, in the Leucite Hills, high Mg isotope ratios (Sun et al., 2021).

5.4. Isotopically intermediate lamproites

The remaining cratonic lamproites exhibit moderately radiogenic Sr (with $\varepsilon Sr_{(i)}$ values ranging from 15 to 110) and unradiogenic but not extreme Nd-Hf isotope compositions ($\varepsilon Nd_{(i)}$ and $\varepsilon Hf_{(i)}$ values down to −15 and −26, respectively) (see Fig. 5). Lamproites originating from various regions such as the Kaapvaal craton (South Africa), Luangwa

valley (Zambia), Bastar craton and Cuddapah basin (India), Aillik Bay (Canada), Sao Francisco craton (Brazil), Argyle and Earaheedy basin (Australia), Baifen (China), Francis (USA), Arkansas (USA), and Gaussberg (Antarctica) fall into this category, and comprise >40% of the lamproite data compilation (see Supplementary Table 1a). In comparison to OIBs and archetypal kimberlites, these lamproites show more geochemically-enriched isotopic compositions (Fig. 5). Furthermore, lamproites from the Kaapvaal craton and Gaussberg (which extend to the lowest Nd-Hf isotopes in this group), exhibit greater enrichment in LILEs and REEs compared to kimberlites (Fig. 4d), but are less enriched relative to the Smoky Butte or Leucite Hills (end-member 3) and West Kimberley lamproites (end-member 2; Fig. 4d). In addition, the Gaussberg lamproites possess some of the highest SiO_2, Al_2O_3, and K_2O contents (Figs. 2, 6) of cratonic lamproites globally.

Considering that for the Kaapvaal lamproites, contribution by a convective-mantle melt component has been previously established (Sarkar et al., 2022, 2023), we attempted to model the isotopic variations observed in this group of lamproites with isotopically intermediate compositions by mixing a melt with PREMA-like isotopic features and MARID (see Table 3 and Supplementary Table 3). However, we cannot rule out that at least some of these lamproites might have originated by melting of metasomatised peridotites at the bottom of the lithosphere (e.g., Foley, 1992; Tappe et al., 2007, 2023). A combination of PREMA-derived melt (10%-40%) and MARID (60%-90%) at 180 Ma matches the isotopic composition of some of these isotopically intermediate lamproites (Fig. 8a-d). On the other hand, these mixing models fail to reproduce the isotopic variations of the older lamproites in this group (i.e. with ages exceeding 500 Ma) such as Argyle, Earaheedy Basin, Bastar Craton, and Cuddapah Basin (see Fig. 8e, 8f), which are rather explained by mixtures of PREMA-like melts with 70–90% of theoretical phlogopite-bearing peridotite components (Enriched components B and C) (Fig. 9a-f). As for the previous mixing models, the very high input from assimilated mica-bearing components (70–90%) can only be achieved through selective rather than bulk assimilation. The intermediate levels of SiO_2, Al_2O_3, K_2O, and TiO_2 (Figs. 2 and 6), along with intermediate enrichment in trace elements (Figs. 7, 9) in these lamproites align with lesser contribution from a phlogopite-bearing component compared to the most extreme major and trace element compositions recorded by lamproites defining the most extreme end-members 2 and 3 (Gaussberg being an exception as also shown by its very low $\varepsilon Nd_{(i)}$ and $\varepsilon Hf_{(i)}$ values; Fig. 5). Nevertheless, all the employed mixing models collectively support or, at least, do not negate the notion that some asthenospheric input is probably required for the genesis of these isotopically intermediate lamproites (see also Murphy et al., 2002; Jaques et al., 2018; Sarkar et al., 2022, 2023). This is also consistent with the negative Zr-Hf anomalies observed in Kaapvaal lamproites, a characteristic also found in melts generated from carbonated peridotites, such as kimberlites (Fig. 4d). In addition, the Os isotope compositions of carbonate-rich olivine lamproites (e.g. Kaapvaal lamproites) show values (median $\gamma Os = -1.4$) comparable to those of kimberlites (median $\gamma Os = -1.8$) (Giuliani et al., 2024), providing additional support for convecting mantle input (as also depicted in our mixing models) in the genesis of cratonic lamproites. However, we cannot entirely rule out that in some cases, the lamproites might be generated solely by melting of metasomatised lithospheric mantle material.

5.5. *Implication for the global occurrence of strongly metasomatised domains in the sub-continental lithospheric mantle*

An inspection of lamproites with highly geochemically-enriched compositions corresponding to end-members 2 and 3, but also some isotopically intermediate localities (e.g., Gaussberg) reveals an intriguing spatiotemporal pattern. The most extreme isotopic compositions (i.e. most radiogenic Sr and unradiogenic Nd-Hf isotopic compositions) including Cenozoic West Kimberley, Smoky Butte, Bear Gulch (Montana), Leucite Hills, Prairie Creek (Arkansas), Gaussberg (Antarctica) and a subset of Kaapvaal are found exclusively in samples younger than 200 Ma with the exception of Sisimiut in West Greenland (~1200 Ma) (Fig. 10). These occurrences are localized in Australia (Cenozoic West Kimberley), North America (Smoky Butte, Bear Gulch (Montana), Leucite Hills, Prairie Creek), South Africa (Kaapvaal), and Antarctica (Gaussberg). In detail, Cenozoic West Kimberley lamproites (around 20 Ma) exhibit the highest radiogenic Sr isotopic composition among global lamproites (Figs. 5, 10a, 10b). In contrast, lamproites from localities in North America, Antarctica and South Africa (plus Sisimiut in West Greenland) have the most unradiogenic Nd and Hf values (Fig. 5, 10c-f). Apart from these isotopically extreme lamproites, more geochemically depleted, i.e., end-member 1 lamproites (Wajrakarur, Melville; having Sr-Nd-Hf compositions close to BSE), are temporarily restricted between 1.2–0.5 Ga (Fig. 10). Considering the different origin and make-up of the extreme geochemically-enriched components examined in this study, which most likely reflect metasomatised lithospheric mantle lithologies, this distribution reflects a strong "provinciality" in the radiogenic isotope systematics of cratonic lamproites. In other words, regional variations in SCLM metasomatism perhaps combined with radiogenic ingrowth are key factors that lead to the formation of lamproites with extreme isotopic compositions. Mitchell (2020, 2021) proposed a similar hypothesis based on the mineralogical composition of global cratonic lamproites, suggesting that lamproites exhibit a wide range of modal mineralogy due to the numerous phases that can crystallize from marginally different lamproitic magmas, which are themselves unique to different regions. Yet, we have only employed isotopic compositions of four different enriched lithospheric assemblages (two from MARIDs and two from different subducted inputs) in our theoretical models (Fig. 9) to explain different end-member lamproites. This is because modeling a separate scenario for each lamproite province would result in an excessively long discussion and extend beyond the scope of this work.

An in-depth analysis of the distinct end-member isotopic signatures and mixing models highlights variations in the lithospheric metasomes required for each lamproite group. These variations are also reflected in the mineralogy and the major element compositions of the isotopically distinct lamproite groups. Specifically, isotopically depleted lamproites (e.g., Wajrakarur; end-member 1) require a minor contribution from phlogopite-clinopyroxene-bearing lithosphere (Figs. 8, 9), assimilated by melts derived from asthenospheric carbonated peridotite. This results in lower SiO_2 and K_2O contents (Fig. 6) and elevated carbonate phases in their groundmass mineralogy. In contrast, isotopically intermediate lamproites (e.g., Kaapvaal lamproites) require a comparatively higher contribution from a phlogopite-clinopyroxene-rich lithospheric component (Fig. 9), consistent with their intermediate SiO_2 and K_2O levels (Fig. 6) and the abundant presence of phlogopite and diopside in their mineralogy. Additionally, Cenozoic West Kimberley lamproites (end-member 2) likely require a metasomatized peridotite enriched in phlogopite and clinopyroxene (±K-richterite), along with ilmenite and rutile. This metasomatic assemblage corresponds to their elevated TiO_2, SiO_2, and K_2O contents, as well as their mineralogy, which features Ti-phlogopite, leucite, K-richterite, and accessory phases such as ilmenite and Ti-rich minerals like priderite. On the other hand, end-member 3 lamproites (e.g., Leucite Hills) appear to require a similar phlogopite- and K-richterite-bearing SCLM but likely lack ilmenite and rutile (Fig. 9). This results in comparable elevated SiO_2 and K_2O contents but moderate to low TiO_2 levels (except for Smoky Butte) (Fig. 6) and a corresponding absence of Ti-bearing phases in their mineralogy. Moreover, the inverse correlation between Nd isotopes and K_2O contents (Fig. 6d) suggests that isotopically extreme lamproites (with highly negative $\varepsilon Nd_{(i)}$ values) interacted with SCLM containing a greater abundance of phlogopite compared to the isotopically depleted lamproites. This relationship further reinforces the link between regional variations in metasomatic mineralogy and the corresponding isotopic compositions and geochemical characteristics of the different end-member lamproites.

This study thus highlights the significance of cratonic lamproites in understanding extreme metasomatism of the SCLM and their corresponding mineralogical variations over considerable timescales. Lamproites are particularly important in this regard because occurrences of MARID rocks or similarly strongly metasomatised peridotites are largely restricted to the Kaapvaal craton (Dawson and Smith, 1977; Waters, 1987; Stiefenhofer et al., 1997; Gregoire et al., 2002 Fitzpayne et al., 2018, 2019), and rare elsewhere (Peterson and Le Cheminant, 1993; Wagner et al., 1996). They hence provide a more extensive perspective on the occurrence and composition of geochemically enriched domains in the lithospheric component compared to the limited record provided by metasomatised mantle xenoliths.

6. Concluding remarks on the genesis of cratonic lamproites

This work reports new Hf isotopic compositions along with Sr-Nd isotopes and major and trace element geochemistry for 61 lamproites to improve our understanding of the origin of these magmas. By integrating these new results with existing data, this work examines the nature of potential mantle components involved in the genesis of cratonic lamproites. Convective-mantle melts are likely to contribute substantially to lamproites in some localities (e.g., Wajrakarur) where the observed moderately geochemically-depleted Sr-Nd-Hf isotopes are indistinguishable from those of (coeval) kimberlites. Conversely, there are cases (e.g., Smoky Butte, Sisimiut) for which there is little, if any, isotopic evidence of convective mantle contribution. Nonetheless, our binary mixing models collectively indicate that mixing between a lithospheric component and an asthenospheric component is a common genetic process for several global lamproites. Further, it is apparent that variations in the composition of the apparently ubiquitous metasomatised lithospheric mantle component combined with heterogeneity in mixing proportions of convective-mantle and lithospheric components play a crucial role in generating distinct isotopic flavours in lamproites from each region. These effects impart a strong "provinciality" in the radiogenic isotope systematics of cratonic lamproites similar to what previously documented based on their mineralogy (Mitchell, 2020, 2021). Regional variations in SCLM composition and metasomatic mineralogy also lead to significant heterogeneity in lamproite SiO_2, Al_2O_3, K_2O, and TiO_2 contents, as well as mineral abundances, along with elevated levels of LILE and LREE, mirroring the extreme isotopic compositions observed in lamproites (Figs. 5, 6, 7). This study underscores the potential of binary mixing models in explaining isotopic variations alongside major and trace element trends, as well as in developing petrogenetic models for alkaline magmas. To further test the proposed petrogenetic scenarios for lamproites, thermodynamic modeling should be pursued as a next step to enhance our understanding of the source constituents of these unusual, yet petrologically important magmas.

Understanding the composition of the mantle components involved in the petrogenesis of lamproites holds significant implications for comprehending intraplate magmatism and lithospheric mantle metasomatism. For instance, delaminated metasomatised lithospheric mantle (as represented by mantle xenoliths and xenocrysts entrained in kimberlites and lamproites) similar to that tapped by the most isotopically-extreme lamproites could mix with convective mantle components to explain EM signatures in some OIBs (e.g., Hawkesworth et al., 1984). In this regard, cratonic lamproites offer a significantly broader perspective on the composition of strongly metasomatised SCLM when compared to mantle xenoliths. In addition, integrating Pb isotopes with Sr-Nd-Hf isotopes would be an important direction to understand these unique rocks. Ongoing and future studies of stable isotopes in cratonic lamproites (Sun et al., 2021; Liu et al., 2022; Chen et al., 2024), especially those of alkali and transitional metal elements, will provide additional insights into the nature and origin of geochemically-enriched components involved in the genesis of lamproites including fluids which have been modifying the sub-continental lithospheric mantle for the last 2 Gyr.

CRediT authorship contribution statement

Soumendu Sarkar: Writing – review & editing, Writing – original draft, Methodology, Investigation, Formal analysis, Data curation, Conceptualization. **Hayden Dalton:** Writing – review & editing, Visualization, Supervision, Conceptualization. **Andrea Giuliani:** Writing – review & editing, Visualization, Supervision, Formal analysis, Conceptualization. **David Phillips:** Writing – review & editing, Visualization, Supervision, Conceptualization. **D. Graham Pearson:** Writing – review & editing, Formal analysis. **Geoff M. Nowell:** Writing – review & editing, Formal analysis. **Jon D. Woodhead:** Writing – review & editing, Formal analysis. **Janet Hergt:** Writing – review & editing, Supervision. **Roland Maas:** Writing – review & editing, Methodology, Formal analysis. **A. Lynton Jaques:** Writing – review & editing. **N.V. Chalapathi Rao:** Writing – review & editing. **Yaakov Weiss:** Writing – review & editing. **Sujoy Ghosh:** Writing – review & editing, Supervision.

Data availability

All the new analysed data presented in this study are available in EarthChem Library (Sarkar, S., Hayden, D., Giuliani, A., Phillips, D., Graham Pearson, D., Nowell, G.M., Woodhead, J.D., Hergt, J., Maas, R., Lynton Jaques, A., Chalapathi Rao, N.V., Weiss, Y., Ghosh, S., 2025. Sr-Nd-Hf, major and trace element compositions of cratonic lamproites, Version 1.0. Interdisciplinary Earth Data Alliance (IEDA). http://doi.org/10.60520/IEDA/113512).

Declaration of competing interest

The authors declare that they have no known competing financial interests or personal relationships that could have appeared to influence the work reported in this paper.

Acknowledgements

This work was performed in part at the Trace Analysis for Chemical, Earth and Environmental Sciences (TrACEES) Platform at the University of Melbourne. We thank David Muphy and Jian-Qiang Liu for providing access to the Gaussberg samples, analysed in this study. Senan Oesch is thanked for his help with XRF analysis and Angus Fitzpayne for undertaking the trace element and isotopic analyses at ETH Zurich. Alan Greig kindly undertook trace element analysis at the University of Melbourn. S. Sarkar's Ph.D. research was supported by a Melbourne Research Scholarship and the Ministry of Human Resource Development, Government of India. Reviews by Marthae Klöcking, Jörg Geldmacher, Hugh O'Brien and two anonymous referees, and editorial input of Dimitri Ionov, Jeff Catalano and Hailiang Dong have substantially improved the clarity of this work.

Appendix A. Supplementary material

The supplementary material for this article includes the following: Supplementary Table 1, which provides a global Sr-Nd-Hf isotope, major, and trace element compilation of cratonic lamproites; Supplementary Table 2, detailing Sr-Nd-Hf isotope, major, and trace element compositions for the analysed samples in this study, along with standard details; and Supplementary Table 3, which outlines all the modelling parameters used in the binary mixing models presented in Figures 8 and

9. The Supplementary document provides 4 figures (Fig. S1 to S4). Supplementary material to this article can be found online at https://doi.org/10.1016/j.gca.2025.02.014.

References

Adams, J.V., Jackson, M.G., Spera, F.J., Price, A.A., Byerly, B.L., Seward, G., Cottle, J.M., 2021. Extreme isotopic heterogeneity in Samoan clinopyroxenes constrains sediment recycling. Nat. Commun. 12 (1), 1234.

Becker, M., Roex, A.P.L., 2006. Geochemistry of South African on-and off-craton, Group I and Group II kimberlites: petrogenesis and source region evolution. J. Petrol. 47 (4), 673–703.

Begemann, F., Ludwig, K.R., Lugmair, G.W., Min, K., Nyquist, L.E., Patchett, P.J., Renne, P.R., Shih, C.Y., Villa, I.M., Walker, R.J., 2001. Call for an improved set of decay constants for geochronological use. Geochim. Cosmochim. Acta 65, 111–121.

Blichert-Toft, J., Chauvel, C., Albarède, F., 1997. Separation of Hf and Lu for high-precision isotope analysis of rock samples by magnetic sector-multiple collector ICP-MS. Contrib. Miner. Petrol. 127 (3), 248–260.

Blichert-Toft, J., Frey, F.A., Albarede, F., 1999. Hf isotope evidence for pelagic sediments in the source of Hawaiian basalts. Science 285 (5429), 879–882.

Bouvier, A., Vervoort, J.D., Patchett, P.J., 2008. The Lu–Hf and Sm–Nd isotopic composition of CHUR: constraints from unequilibrated chondrites and implications for the bulk composition of terrestrial planets. Earth Planet. Sci. Lett. 273 (1–2), 48–57.

Carlson, R.W., Irving, A.J., 1994. Depletion and enrichment history of subcontinental lithospheric mantle: an Os, Sr, Nd and Pb isotopic study of ultramafic xenoliths from the northwestern Wyoming Craton. Earth Planet. Sci. Lett. 126 (4), 457–472.

Chalapathi Rao, N.V., Lehmann, B., 2011. Kimberlites, flood basalts and mantle plume: New insights from the Deccan large igneous province. Earth Sci. Rev. 107, 315–324.

Chalapathi Rao, N.V., Burgess, R., Nanda, P., Choudhary, A.K., Sahoo, S., Lehmann, B., Chahong, N., 2016. Petrology, 40Ar/39Ar age, Sr-Nd isotope systematics, and geodynamic significance of an ultrapotassic (lamproitic) dyke with affinities to kamafugite from the easternmost margin of the Bastar Craton. India. Miner. Petrol. 110 (2), 269–293.

Chalapathi Rao, N.V., Gibson, S.A., Pyle, D.M., Dickin, A.P., 2004. Petrogenesis of Proterozoic lamproites and kimberlites from the Cuddapah Basin and Dharwar craton, southern India. J. Petrol. 45 (5), 907–948.

Chalapthi Rao, N.V., Wu, F.Y., Mitchell, R.H., Li, Q.L., Lehmann, B., 2013. Mesoproterozoic U–Pb ages, trace element and Sr–Nd isotopic composition of perovskite from kimberlites of the Eastern Dharwar craton, southern India: Distinct mantle sources and a widespread 1.1 Ga tectonomagmatic event. Chem. Geol. 353, 48–64.

Chauvel, C., Hofmann, A.W., Vidal, P., 1992. HIMU-EM: the French Polynesian connection. Earth Planet. Sci. Lett. 110 (1–4), 99–119.

Chauvel, C., Lewin, E., Carpentier, M., Arndt, N.T., Marini, J.C., 2008. Role of recycled oceanic basalt and sediment in generating the Hf–Nd mantle array. Nat. Geo. 1 (1), 64–67.

Chen, C., Foley, S.F., Shcheka, S.S., Liu, Y., 2024. Copper isotopes track the Neoproterozoic oxidation of cratonic mantle roots. Nat. Commun. 15 (1), 4311.

Coe, N., Le Roex, A., Gurney, J., Pearson, D.G., Nowell, G., 2008. Petrogenesis of the Swartruggens and Star Group II kimberlite dyke swarms, South Africa: constraints from whole rock geochemistry. Contrib. Miner. Petrol. 156 (5), 627–652.

Dalton, H., Giuliani, A., Hergt, J., Phillips, D., O'Brien, H., Ballmer, M.D., Maas, R., Woodhead, J., 2022. Geodynamic and isotopic constraints on the genesis of kimberlites, lamproites and related magmas from the Finnish segment of the Karelian craton. Geochem. Geophys. Geosyst. 23 (8), e2021GC010324.

Dalton, H., Giuliani, A., O'Brien, H., Phillips, D., Hergt, J., Maas, R., 2019. Petrogenesis of a hybrid cluster of evolved kimberlites and ultramafic lamprophyres in the Kuusamo area. Finland. J. Petrol. 60 (10), 2025–2050.

Das, H., Kobussen, A.F., Webb, K.J., Phillips, D., Maas, R., Soltys, A., Rayner, M.J., Howell, D., 2018. The Bunder Diamond Project, India: Geology, geochemistry, and age of the Saptarshi lamproite Pipes. In: Davy, A.T., Smith, C.B., Helmstaedt, H.H., Jaques, A.L., Gurney, J.J. (Eds.), Geoscience and Exploration of the Argyle, Bunder, Diavik, and Murowa Diamond Deposits. Allen Press Inc., Kansas, pp. 201–222.

Davies, G.R., Stolz, A.J., Mahotkin, I.L., Nowell, G.M., Pearson, D.G., 2006. Trace element and Sr–Pb–Nd–Hf isotope evidence for ancient, fluid-dominated enrichment of the source of Aldan Shield lamproites. J. Petrol. 47 (6), 1119–1146.

Dawson, J.B., 1980. Kimberlites and their xenoliths. Springer, Berlin.

Dawson, J.B., Smith, J.V., 1977. The MARID (mica-amphibole-rutile-ilmenite-diopside) suite of xenoliths in kimberlite. Geochim. Cosmochim. Acta 41 (2), 309–323.

Desem, C.U., Woodhead, J., de Caritat, P., Maas, R., Champion, D.C., Dosseto, A., Wainwright, A., Carr, G., 2025. The Pb, Sr and Nd isotopic composition of the upper continental crust: an Australian perspective. Chem. Geol. 672, 122503.

Dowall, D.P., Pearson, D.G., Nowell, G.M., 2003. Chemical preconcentration procedures for high-precision analysis of Hf–Nd–Sr isotopes in geological materials by plasma ionisation multi-collector mass spectrometry (PIMMS) techniques. In: Holland, J.G., Tanner, S.D. (Eds.), Plasma Source Mass Spectrometry: Applications and Emerging Technologies. Royal Society of Chemistry, Cambridge, pp. 321–337.

Eggins, S.M., Woodhead, J.D., Kinsley, L.P.J., Mortimer, G.E., Sylvester, P., McCulloch, M.T., Hergt, J.M., Handler, M.R., 1997. A simple method for the precise determination of ≥ 40 trace elements in geological samples by ICPMS using enriched isotope internal standardisation. Chem. Geol. 134 (4), 311–326.

Fitzpayne, A., Giuliani, A., Hergt, J., Phillips, D., Janney, P., 2018. New geochemical constraints on the origins of MARID and PIC rocks: Implications for mantle metasomatism and mantle-derived potassic magmatism. Lithos 318–319, 478–493.

Fitzpayne, A., Giuliani, A., Howarth, G.H., Peters, B.J., Fehr, M.A., Maas, R., 2023. Major- , trace-element and Sr-Nd-Hf isotope geochemistry of diamondiferous dykes from Tonguma and Koidu, Sierra Leone: Highly micaceous kimberlites formed by assimilation of metasomatised lithospheric mantle rocks. Chem. Geol. 630, 121475.

Fitzpayne, A., Giuliani, A., Maas, R., Hergt, J., Janney, P., Phillips, D., 2019. Progressive metasomatism of the mantle by kimberlite melts: Sr-Nd-Hf-Pb isotope compositions of MARID and PIC minerals. Earth Planet. Sci. Lett. 509, 15–26.

Foley, S., 1992. Vein-plus-wall-rock melting mechanisms in the lithosphere and the origin of potassic alkaline magmas. Lithos 28, 435–453.

Foley, S.F., Ezad, I.S., 2024. Melting of hydrous pyroxenites with alkali amphiboles in the continental mantle: 2. Trace element compositions of melts and minerals. Geosci. Front. 15 (1), 101692.

Foley, S.F., Ezad, I.S., van der Laan, S.R., Pertermann, M., 2022. Melting of hydrous pyroxenites with alkali amphiboles in the continental mantle: 1. Melting relations and major element compositions of melts. Geosci. Front. 13 (4), 101380.

Foley, S.F., Venturelli, G., Green, D.H., Toscani, L., 1987. The ultrapotassic rocks: Characteristics, classification, and constraints for petrogenetic models. Earth Sci. Rev. 24, 81–134.

Fraser, K.J., Hawkesworth, C.J., 1992. The petrogenesis of group 2 ultrapotassic kimberlites from Finsch Mine. South Africa. Lithos 28 (3–6), 327–345.

Fraser, K.J., Hawkesworth, C.J., Erlank, A.J., Mitchell, R.H., Scott-Smith, B.H., 1985. Sr, Nd and Pb isotope and minor element geochemistry of lamproites and kimberlites. Earth Planet. Sci. Lett. 76, 57–70.

Gale, A., Dalton, C.A., Langmuir, C.H., Su, Y., Schilling, J.G., 2013. The mean composition of ocean ridge basalts. Geochem. Geophys. Geosyst. 14 (3), 489–518.

Gao, M., Foley, S.F., Xu, H., Wang, Y., 2023. Mantle metasomatism induced by water-fluxed melting of subducted continental crust at ultrahigh pressures. Geology 51 (12), 1127–1131.

Gaschnig, R.M., Horan, M.F., Rudnick, R.L., Vervoort, J.D., Fisher, C.M., 2022. History of crustal growth in Africa and the Americas from detrital zircon and Nd isotopes in glacial diamictites. Precambrian Res. 373, 106641.

Giuliani, A., Campeny, M., Kamenetsky, V.S., Afonso, J.C., Maas, R., Melgarejo, J.C., Kohn, B.P., Matchan, E.L., Mangas, J., Gonçalves, A.O., Manuel, J., 2017. Southwestern Africa on the burner: Pleistocene carbonatite volcanism linked to deep mantle upwelling in Angola. Geology 45 (11), 971–974.

Giuliani, A., Dalton, H., Pearson, D.G., 2024. Kimberlites: The deepest geochemical probes of Earth. In: Anbar, A., Weis, D. (Eds.), Treatise on Geochemistry. Third edition, pp. 159–230.

Giuliani, A., Drysdale, R.N., Woodhead, J.D., Planavsky, N.J., Phillips, D., Hergt, J., Griffin, W.L., Oesch, S., Dalton, H., Davies, G.R., 2022. Perturbation of the deep-Earth carbon cycle in response to the Cambrian Explosion. Sci. Adv. 8 (9), eabj1325.

Giuliani, A., Jackson, M.G., Fitzpayne, A., Dalton, H., 2021. Remnants of early Earth differentiation in the deepest mantle-derived lavas. Proc. Natl. Acad. Sci. 118 (1), e2015211118.

Giuliani, A., Pearson, D.G., Soltys, A., Dalton, H., Phillips, D., Foley, S.F., Lim, E., Goemann, K., Griffin, W.L., Mitchell, R.H., 2020. Kimberlite genesis from a common carbonate rich primary melt modified by lithospheric mantle assimilation. Sci. Adv. 6, eaaz0424.

Giuliani, A., Phillips, D., Woodhead, J.D., Kamenetsky, V.S., Fiorentini, M.L., Maas, R., Soltys, A., Armstrong, R.A., 2015. Did diamond-bearing orangeites originate from MARID-veined peridotites in the lithospheric mantle? Nat. Commun. 6, 6837.

Giuliani, A., Schmidt, M.W., Torsvik, T.H., Fedortchouk, Y., 2023. Genesis and evolution of kimberlites. Nat. Rev. Earth Environ. 1–16.

Grégoire, M., Bell, D., Le Roex, A., 2002. Trace element geochemistry of phlogopite-rich mafic mantle xenoliths: their classification and their relationship to phlogopite-bearing peridotites and kimberlites revisited. Contrib. Miner. Petrol. 142, 603–625.

Hart, S.R., Hauri, E.H., Oschmann, L.A., Whitehead, J.A., 1992. Mantle plumes and entrainment: isotopic evidence. Science 256 (5056), 517–520.

Hawkesworth, C.J., Rogers, N.W., Van Calsteren, P.W.C., Menzies, M.A., 1984. Mantle enrichment processes. Nature 311 (5984), 331–335.

Jackson, M.G., Dasgupta, R., 2008. Compositions of HIMU, EM1, and EM2 from global trends between radiogenic isotopes and major elements in ocean island basalts. Earth Planet. Sci. Lett. 276 (1–2), 175–186.

Jackson, M.G., Hart, S.R., Koppers, A.A., Staudigel, H., Konter, J., Blusztajn, J., Kurz, M., Russell, J.A., 2007. The return of subducted continental crust in Samoan lavas. Nature 448 (7154), 684–687.

Jackson, M.G., Jellinek, A.M., 2013. Major and trace element composition of the high $^{3}He/^{4}He$ mantle: Implications for the composition of a nonchonditic Earth. Geochem. Geophys. Geosyst. 14 (8), 2954–2976.

Jaques, A.L., 2024. Petrology, Geochemistry and Mantle Minerals of the Walgidee Hills Lamproite, West Kimberley, Western Australia. J. Petrol. egae040.

Jaques, A.L., Lewis, J.D., Smith, C.B., Gregory, G.P., Ferguson, J., Chappell, B.W., McCulloch, M.T., 1984. The diamond bearing ultrapotassic (lamproitic) rocks of the west Kimberley region. In: Kornprobst, J. (Ed.), Kimberlites and Related Rocks, Proceedings of the Third International Kimberlite Conference. Elsevier Science Publishers, Clermont Ferrand, France, pp. 225–254.

Jaques, A.L., Luguet, A., Smith, C.B., Pearson, D., Yaxley, G.M., Kobussen, A., 2018. Nature of the mantle beneath the Argyle AK1 lamproite pipe: Constraints from mantle xenoliths, diamonds, and lamproite geochemistry, in: Davy, T., et al., (Eds), Geoscience and Exploration of the Argyle, Bunder, Diavik, and Murowa Diamond Deposits: Society of Economic Geologists Special Publication 20, 119–143.

Johnson, M.C., Plank, T., 2000. Dehydration and melting experiments constrain the fate of subducted sediments. Geochemi. Geophys. Geosys. 1 (12).

Kamber, B.S., Greig, A., Schönberg, R., Collerson, K.D., 2003. A refined solution to Earth's hidden niobium: implications for evolution of continental crust and mode of core formation. Precambrian Res. 126, 289–308.
Kjarsgaard, B.A., de Wit, M., Heaman, L.M., Pearson, D.G., Stiefenhofer, J., Janusczcak, N., Shirey, S.B., 2022. A review of the geology of global diamond mines and deposits. Rev. Miner. Geochem. 88 (1), 1–117.
Kogiso, T., Tatsumi, Y., Nakano, S., 1997. Trace element transport during dehydration processes in the subducted oceanic crust: 1. Experiments and implications for the origin of ocean island basalts. Earth Planet, Sci. Lett. 148 (1–2), 193–205.
Konter, J.G., Hanan, B.B., Blichert-Toft, J., Koppers, A.A.P., Plank, T., Staudigel, H., 2008. One hundred million years of mantle geochemical history suggest the retiring of mantle plumes is premature. Earth Planet. Sci. Lett. 275, 285–295.
Liu, J.Q., Chen, L.H., Wang, X.J., Zhang, X.Y., Zeng, G., Erdmann, S., Murphy, D.T., Collerson, K.D., Komiya, T., Krmíček, L., 2022. Magnesium and zinc isotopic evidence for the involvement of recycled carbonates in the petrogenesis of Gaussberg lamproites. Antarctica. Chem. Geol. 609, 121067.
Mahotkin, I.L., 1998. Petrology of the Group 2 kimberlite–olivine lamproite (K2L) series from the Kostomksha area, Karelia, NW Russia. In: Town, C., Africa, S. (Eds.), 7th International Kimberlite Conference, pp. 529–531.
McCulloch, M.T., Jaques, A.L., Nelson, D.R., Lewis, J.D., 1983. Nd and Sr isotopes in kimberlites and lamproites from Western Australia: An enriched mantle origin. Nature 302, 400–403.
McCulloch, M.T., Wasserburg, G.J., 1978. Sm-Nd and Rb-Sr Chronology of Continental Crust Formation: Times of addition to continents of chemically fractionated mantle-derived materials are determined. Science 200 (4345), 1003–1011.
McDonough, W.F., Sun, S.S., 1995. The composition of the Earth. Chem. Geol. 120 (3–4), 223–253.
Meltzer, A., Kessel, R., 2022. The interaction of slab-derived silicic fluid and harzburgite–Metasomatism in the sub cratonic lithospheric mantle. Geochim. Cosmochim. Acta 328, 103–119.
Meltzer, A., Kessel, R., 2023. The metasomatism of sub-cratonic peridotites by a slab-derived fluid–Implications for cratons' evolution. Geochim. Cosmochim. Acta 350, 28–45.
Mirnejad, H., Bell, K., 2006. Origin and source evolution of the Leucite Hills lamproites: evidence from Sr–Nd–Pb–O isotopic compositions. J. Petrol. 47 (12), 2463–2489.
Mitchell, R.H., 1986. Kimberlites: mineralogy, geochemistry, and petrology. Plenum Press, New York.
Mitchell, R.H., 1995. Kimberlites and orangeites. In: Boston, M.A. (Ed.), Kimberlites, Orangeites, and Related Rocks. Springer, pp. 1–90.
Mitchell, R.H., 2020. Igneous rock associations 26. Lamproites, exotic potassic alkaline rocks: a review of their nomenclature, characterization and origins. Geosci. Canada 47 (3), 119–142.
Mitchell, R.H., 2021. Potassic alkaline rocks . Leucitites, lamproites, and kimberlites. In: Alderton, D., Elias, S.A. (Eds.), Encyclopedia of Geology, (2nd Eds). Academic Press, San Diego, California, pp. 215–239.
Mitchell, R.H., Bergman, S.C., 1991. Petrology of lamproites. Plenum Publishing Company, New York, p. 447p.
Murphy, D.T., Collerson, K.D., Kamber, B.S., 2002. Lamproites from Gaussberg, Antarctica: Possible transition zone melts of Archaean subducted sediments. J. Petrol. 43, 981–1001.
Nebel, O., Arculus, R.J., van Westrenen, W., Woodhead, J.D., Jenner, F.E., Nebel-Jacobsen, Y.J., Wille, M., Eggins, S.M., 2013. Coupled Hf–Nd–Pb isotope co-variations of HIMU oceanic island basalts from Mangaia, Cook-Austral islands, suggest an Archean source component in the mantle transition zone. Geochim. Cosmochim. Acta 112, 87–101.
Nelson, D.R., McCulloch, M.T., Sun, S.S., 1986. The origins of ultrapotassic rocks as inferred from Sr, Nd and Pb isotopes: Geochim. Cosmochim. Acta 50, 231–245.
Nowell, G.M., Pearson, D.G., Bell, D.R., Carlson, R.W., Smith, C.B., Kempton, P.D., Noble, S.R., 2004. Hf isotope systematics of kimberlites and their megacrysts: new constraints on their source regions. J. Petrol. 45 (8), 1583–1612.
Nowell, G.M., Pearson, D.G., Kempton, P.D., Irving, A.J., Turner, S., 1998. A Hf isotope study of lamproites: Implications for their origins and relationship to kimberlites. In: Gurney, J.J. (Ed.), International Kimberlite Conference, Extended Abstracts, Volume 7: Cape Town, South Africa, Red Roof Design, pp. 637–639.
O'Brien, H., Tyni, M., 1999. Mineralogy and geochemistry of kimberlites and related rocks from Finland. In: Gurney, J.J., Gurney, J.L., Pascoe, M.D., Richardson, S.H. (Eds.), Proc 7th International Kimberlite Conference, Red Roof Design Cape Town, pp. 625–636.
Ottley, C.J., Pearson, D.G., Irvine, G.J., 2003. A routine method for the dissolution of geological samples for the analysis of REE and trace elements via ICP-MS. In: Holland, J.G., Tanner, S.D. (Eds.), Plasma Source Mass Spectrometry: Applications and Emerging Technologies. The Royal Society of Chemistry, Cambridge, pp. 221–230.
Paton, C., Hergt, J.M., Woodhead, J.D., Phillips, D., Shee, S.R., 2009. Identifying the asthenospheric component of kimberlite magmas from the Dharwar Craton, India. Lithos 112, 296–310.
Pearson, D.G., Scott, J.M., Liu, J., Schaeffer, A., Wang, L.H., van Hunen, J., Szilas, K., Chacko, T., Kelemen, P.B., 2021. Deep continental roots and cratons. Nature 596 (7871), 199–210.
Pearson, D.G., Woodhead, J., Janney, P.E., 2019. Kimberlites as geochemical probes of Earth's mantle. Elements 15, 387–392.
Peterson, T.D., LeCheminant, A.N., 1993. Glimmerite xenoliths in Early Proterozoic ultrapotassic rocks from the Churchill Province. Canadian Miner. 31 (4), 801–819.
Phillips, D., Machin, K.J., Kiviets, G.B., Fourie, L.F., Roberts, M.A., Skinner, E.M.W., 1998. A petrographic and 40Ar/39Ar geochronological study of the Voorspoed kimberlite, South Africa: implications for the origin of group II kimberlite magmatism. South Afr. J. Geol. 101, 299–306.
Plank, T., 2014. The chemical composition of subducting sediments. In: Holland, H.D., Turekian, K.K. (Eds.), Treatise on Geochemistry, (2nd Eds),. Elsevier, pp. 607–629.
Prelević, D., Foley, S.F., Romer, R., Conticelli, S., 2008. Mediterranean Tertiary lamproites derived from multiple source components in postcollisional geodynamics. Geochim. Cosmochim. Acta 72 (8), 2125–2156.
Reddicliffe T.H., Jakimowicz J., Hell A.J., Robins J.A., 2003. The geology, mineralogy, and near surface characteristics of the Ashmore and Seppelt kimberlite clusters, north Kimberley Province, Australia. In: International kimberlite conference: extended abstracts, (8), 5.
Royse, K.R., Kempton, P.D., Darbyshire, D.P.F., 1998. Procedure for the analysis of rubidium–strontium and samarium–neodymium isotopes at the NERC Isotope Geosciences Laboratory. NIGL Report Series 121, 28p.
Rudnick, R.L., Gao, S., 2014. Composition of the continental crust. In: Turekian, H.D., Holland, K.K. (Eds.), Treatise on Geochemistry, (2nd Eds). Elsevier, Oxford, pp. 1–51.
Sarkar, C., Kjarsgaard, B.A., Pearson, D.G., Heaman, L.M., Locock, A.J., Armstrong, J.P., 2018. Geochronology, classification and mantle source characteristics of kimberlites and related rocks from the Rae Craton, Melville Peninsula, Nunavut, Canada. Miner. Petrol. 112, 653–672.
Sarkar, S., Giuliani, A., Dalton, H., Phillips, D., Ghosh, S., Misev, S., Maas, R., 2023. Derivation of lamproites and kimberlites from a common evolving source in the convective mantle: the case for southern african 'transitional kimberlites'. J. Petrol. 64 (7), egad043.
Sarkar, S., Giuliani, A., Ghosh, S., Phillips, D., 2021. Petrogenesis of coeval lamproites and kimberlites from the Wajrakarur field, southern India: New insights from olivine compositions. Lithos 406–407, 106524.
Sarkar, S., Giuliani, A., Phillips, D., Howarth, G.H., Ghosh, S., Dalton, H., 2022. Sublithospheric melt input in cratonic lamproites. Geology 50 (11), 1296–1300.
Scherer, E., Munker, C., Mezger, K., 2001. Calibration of the lutetium-hafnium clock. Science 293 (5530), 683–687.
Shaikh, A.M., Kumar, S.P., Patel, S.C., Thakur, S.S., Ravi, S., Behera, D., 2018. The P3 kimberlite and P4 lamproite, Wajrakarur kimberlite field, India: Mineralogy, and major and minor element compositions of olivines as records of their phenocrystic vs. xenocrystic origin. Miner. Petrol. 112, 609–624.
Smith, C., 1983. Pb, Sr and Nd isotopic evidence for sources of southern African Cretaceous kimberlites. Nature 304, 51–54.
Stachel, T., Harris, J.W., Hunt, L., Muehlenbachs, K. and Kobussen, A.F., 2018. Argyle diamonds: How subduction along the Kimberley Craton edge generated the world's biggest diamond deposit, in: Davy, T., et al. (Eds), Geoscience and Exploration of the Argyle, Bunder, Diavik, and Murowa Diamond Deposits. Society of Economic Geologists Special Publication 20, 145–167.
Stiefenhofer, J., Viljoen, K.S., Marsh, J.S., 1997. Petrology and geochemistry of peridotite xenoliths from the Letlhakane kimberlites. Botswana. Contrib. Miner. Petrol. 127, 147–158.
Stracke, A., Bizimis, M., Salters, V.J., 2003. Recycling oceanic crust: Quantitative constraints. Geochem. Geophys. Geosyst. 4 (3), 8003.
Stracke, A., Willig, M., Genske, F., Béguelin, P., Todd, E., 2022. Chemical geodynamics insights from a machine learning approach. Geochem. Geophys. Geosyst. 23 (10).
Sun, Y., Teng, F.Z., Pang, K.N., Ying, J.F., Kuehner, S., 2021. Multistage mantle metasomatism deciphered by Mg− Sr− Nd− Pb isotopes in the Leucite Hills lamproites. Contrib. Miner. Petrol. 176 (6), 45.
Sun, Y., Ying, J., Zhou, X., Chu, Z., Su, B., 2014. Geochemistry of ultrapotassic volcanic rocks in Xiaogulihe NE China: implications for the role of ancient subducted sediments. Lithos 208, 53–66.
Tainton, K.M., McKenzie, D.A.N., 1994. The generation of kimberlites, lamproites, and their source rocks. J. Petrol. 35 (3), 787–817.
Tappe, S., Foley, S.F., Kjarsgaard, B.A., Romer, R.L., Heaman, L.M., Stracke, A., Jenner, G.A., 2008. Between carbonatite and lamproite—Diamondiferous Torngat ultramafic lamprophyres formed by carbonate-fluxed melting of cratonic MARID-type metasomes. Geochim. Cosmochim. Acta 72, 3258–3286.
Tappe, S., Foley, S.F., Stracke, A., Romer, R.L., Kjarsgaard, B.A., Heaman, L.M., Joyce, N., 2007. Craton reactivation on the Labrador Sea margins: 40Ar/39Ar age and Sr–Nd–Hf–Pb isotope constraints from alkaline and carbonatite intrusives. Earth Planet. Sci. Lett. 256, 433–454.
Tappe, S., Pearson, G.D., Kjarsgaard, B.A., Nowell, G., Dowall, D., 2013. Mantle transition zone input to kimberlite magmatism near a subduction zone: Origin of anomalous Nd– Hf isotope systematics at Lac de Gras. Canada. Earth Planet. Sci. Lett. 371–372, 235–251.
Tappe, S., Ngwenya, N.S., Stracke, A., Romer, R.L., Glodny, J., Schmitt, A.K., 2023. Plume–lithosphere interactions and LIP-triggered climate crises constrained by the origin of Karoo lamproites. Geochim. Cosmochim. Acta 350, 87–105.
Tappe, S., Smart, K., Torsvik, T., Massuyeau, M., de Wit, M., 2018. Geodynamics of kimberlites on a cooling Earth: clues to plate tectonic evolution and deep volatile cycles. Earth Planet. Sci. Lett. 484, 1–14.
Tappe, S., Stracke, A., van Acken, D., Strauss, H., Luguet, A., 2020. Origins of kimberlites and carbonatites during continental collision–insights beyond decoupled Nd-Hf isotopes. Earth Sci. Rev. 208, 103287.
Thirlwall, M.F., 1991. Long-term reproducibility of multicollector Sr and Nd isotope ratio analysis. Chem. Geol. 94 (2), 85–104.
Tingey, R.J., McDougall, I., Gleadow, A.J.W., 1983. The age and mode of formation of Gaussberg, Antarctica. J. Geol. Soci. Australia 30, 241–246.
Vance, D., Thirlwall, M.F., 2002. An assessment of mass discrimination in MC-ICPMS using Nd isotopes. Chem. Geol. 185, 227–240.

Van de Löcht, J., Hoffmann, J.E., Rosing, M.T., Sprung, P., Münker, C., 2020. Preservation of Eoarchean mantle processes in ~3.8 Ga peridotite enclaves in the Itsaq Gneiss Complex, southern West Greenland. Geochim. Cosmochim. Acta 280, 1–25.
Vervoort, J.D., Patchett, P.J., Söderlund, U., Baker, M., 2004. Isotopic composition of Yb and the determination of Lu concentrations and Lu/Hf ratios by isotope dilution using MC- ICPMS. Geochem. Geophys. Geosyst. 5, Q1102.
Vervoort, J.D., Plank, T., Prytulak, J., 2011. The Hf–Nd isotopic composition of marine sediments. Geochim. Cosmochim. Acta 75 (20), 5903–5926.
Villa, I.M., De Bièvre, P., Holden, N.E., Renne, P.R., 2015. IUPAC-IUGS recommendation on the half life of 87Rb. Geochim. Cosmochim. Acta 164, 382–385.
Wagner, C., Deloule, E., Mokhtari, A., 1996. Richterite-bearing peridotites and MARID-type inclusions in lavas from North Eastern Morocco: mineralogy and D/H isotopic studies. Contrib. Miner. Petrol. 124, 406–421.
Waight, T.E., Baker, J., Willigers, B., 2002. Rb isotope dilution analyses by MC-ICPMS using Zr to correct for mass fractionation: towards improved Rb–Sr geochronology? Chem. Geol. 186, 99–116.
Wang, C., Zhang, Z., Giuliani, A., Cai, R., Cheng, Z., Liu, J., 2022. New insights into the mantle source of a large igneous province from highly siderophile element and Sr-Nd- Os isotope compositions of carbonate-rich ultramafic lamprophyres. Geochim. Cosmochim. Acta 326, 77–96.
Wang, C., Zhang, Z., Giuliani, A., Cheng, Z., Liu, B., Kong, W., 2021. Geochemical and O–C–Sr–Nd isotopic constraints on the petrogenetic link between aillikites and carbonatites in the Tarim large igneous province. J. Petrol. 62 (5), egab017.
Waters, F.G., 1987. A suggested origin of MARID xenoliths in kimberlites by high pressure crystallization of an ultrapotassic rock such as lamproite. Contrib. Miner. Petrol. 95, 523–533.
Weaver, B.L., 1991. The origin of ocean island basalt end-member compositions: trace element and isotopic constraints. Earth Planet. Sci. Lett. 104 (2–4), 381–397.
Woolley, A.R., Bergman, S.C., Edgar, A.D., Le Bas, M.J., Mitchell, R.H., Rock, N.M., Scott Smith, B.H., 1996. Classification of lamprophyres, lamproites, kimberlites, and the kalsilitic, melilitic, and leucitic rocks. Canadian Miner. 34, 175–186.
Woodhead, J., Hergt, J., Giuliani, A., Maas, R., Phillips, D., Pearson, D.G., Nowell, G., 2019. Kimberlites reveal 2.5-billion-year evolution of a deep, isolated mantle reservoir. Nature 573, 578–581.
Workman, R.K., Hart, S.R., 2005. Major and trace element composition of the depleted MORB mantle (DMM). Earth Planet. Sci. Lett. 231 (1–2), 53–72.
Wunder, B., Melzer, S., 2003. Experimental evidence on phlogopitic mantle metasomatism induced by phengite dehydration. European J. Miner. 15 (4), 641–647.
Wyatt, B.A., Sumpton, J.D.H., Shee, S.R., Smith, T.W., 1998. Kimberlites in the forrest river area, Kimberley region, Western Australia. In International Kimberlite Conference: Extended Abstracts 7, 971–973.
Xiang, L., Zheng, J.P., Zhai, M.G., Siebel, W., 2020. Geochemical and Sr–Nd–Pb isotopic constraints on the origin and petrogenesis of Paleozoic lamproites in the southern Yangtze Block South China. Contrib. Miner. Petrol. 175, 29.
Xu, J.Y., Giuliani, A., Li, Q.L., Lu, K., Melgarejo, J.C., Griffin, W.L., 2021. Light oxygen isotopes in mantle-derived magmas reflect assimilation of sub-continental lithospheric mantle material. Nat. Commun. 12 (1), 6295.
Yaxley, G.M., Anenburg, M., Tappe, S., Decree, S., Guzmics, T., 2022. Carbonatites: classification, sources, evolution, and emplacement. Annual Rev. Earth Planet. Sci. 50, 261–293.
Zindler, A., Hart, S., 1986. Chemical geodynamics. Annual Rev. Earth Planet. Sci. 14, 493–571.